PAPER • **OPEN ACCESS**

Efficient modeling of electron kinetics under influence of externally applied electric field in magnetized weakly ionized plasma

To cite this article: Reza Janalizadeh *et al* 2023 *Plasma Sources Sci. Technol.* **32** 075004

OPEN ACCESS
IOP Publishing
Plasma Sources Science and Technology
Plasma Sources Sci. Technol. **32** (2023) 075004 (16pp)
https://doi.org/10.1088/1361-6595/acdaf1

Efficient modeling of electron kinetics under influence of externally applied electric field in magnetized weakly ionized plasma

Reza Janalizadeh*, **Zaid Pervez and Victor P Pasko**

Communications and Space Sciences Laboratory, Department of Electrical Engineering, The Pennsylvania State University, University Park, PA 16802, United States of America

E-mail: reza.j@psu.edu

Received 6 March 2023, revised 5 May 2023
Accepted for publication 2 June 2023
Published 7 July 2023

Abstract

We present a theory based on the conventional two-term (i.e. Lorentzian) approximation to the exact solution of the Boltzmann equation in non-magnetized weakly ionized plasma to efficiently obtain the electron rate and transport coefficients in a magnetized plasma for an arbitrary magnitude and direction of applied electric field $\vec{E}$ and magnetic field $\vec{B}$. The proposed transcendental method does not require the two-term solution of the Boltzmann equation in magnetized plasma, based on which the transport parameters vary as a function of the reduced electric field E/N, reduced electron cyclotron frequency ω_{ce}/N, and angle $\angle\vec{E},\vec{B}$ between $\vec{E}$ and $\vec{B}$ vectors, where N is the density of neutrals. Comparisons between the coefficients derived from BOLSIG+'s solution (obtained via the two-term expansion when $\vec{B} \neq 0$) and coefficients of the presented method are illustrated for air, a mixture of molecular hydrogen (H_2) and helium (He) representing the giant gas planets of the Solar System, and pure carbon dioxide (CO_2). The new approach may be used in the modeling of magnetized plasma encountered in the context of transient luminous events, e.g. sprite streamers in the atmosphere of Earth and Jupiter, in modeling the propagation of lightning's electromagnetic pulses in Earth's ionosphere, and in various laboratory and industrial applications of nonthermal plasmas.

Supplementary material for this article is available online

Keywords: electron energy distribution function, electron transport and rate coefficients, Hall parameter, magnetized plasma, nonthermal plasma, weakly ionized plasma, gas discharge

1. Introduction

Starikovskiy *et al* (2021) reported the first plasma fluid model for magnetized streamer discharges. The authors studied streamer propagation parallel to a magnetic field in pure CO_2. The motivations for this study included the significant interest in the energy generation cycle of magnetohydrodynamic generators, the possible utilization of CO_2 in alternative renewable energy sources, and the use of CO_2 as an alternative to SF_6 for insulation in high-voltage transmission and distribution networks due to its lower environmental impact (e.g. Hernandez-Avila *et al* 2002, Seeger *et al* 2016, Starikovskiy *et al* 2021).

Transient luminous events are a set of frequently observed lightning-induced optical phenomena that were serendipitously discovered by Franz *et al* (1990). In particular,

* Author to whom any correspondence should be addressed.

a transient luminous event referred to as an elve (e.g. Fukunishi *et al* 1996), which is the optical manifestation of the ionosphere interacting with a lightning electromagnetic pulse, occurs at lower ionospheric altitudes, i.e. ∼100 km, in the Earth's atmosphere. The Earth's geomagnetic field plays an important role in the structure of elves. For instance, Nagano *et al* (2003) attributed the asymmetry exhibited in the shape of elves to the Earth's geomagnetic field. A three-dimensional finite difference time domain model that accounts for the effects of electron heating on electron mobility and for the asymmetry of elves due to the geomagnetic field was reported in Marshall (2009), Marshall *et al* (2010). This asymmetry was not observed in studies that excluded Earth's magnetic field (Barrington-Leigh *et al* 2001, Veronis *et al* 2001, Kuo *et al* 2007, Liu *et al* 2017, Pérez-Invernón *et al* 2018).

Following the first observation of possible transient luminous events on Jupiter reported by Giles *et al* (2020), Janalizadeh and Pasko (2023) developed a numerical model for the modeling of magnetized streamers in the presence of Jupiter's strong magnetic field. Similar to Starikovskiy *et al* (2021), streamer propagation was considered in a cylindrical coordinate system, where the magnetic field was parallel to the axis, and magnetized streamers were studied in the molecular hydrogen and helium-dominated atmosphere of Jupiter.

Following Starikovskiy *et al* (2021), in Janalizadeh and Pasko (2023), BOLSIG+ (Hagelaar and Pitchford 2005) was used to calculate the electron transport and rate coefficients as a function of the reduced electric field E/N, reduced electron cyclotron frequency ω_{ce}/N, and angle $\angle\vec{E},\vec{B}$ between the applied electric field $\vec{E}$ and magnetic field $\vec{B}$ vectors. In Janalizadeh and Pasko (2023, and references therein) it is demonstrated that in the presence of a magnetic field transport parameters of a weakly ionized plasma vary as a function of $(E/N,\omega_{ce}/N,\angle\vec{E},\vec{B})$. As done in Starikovskiy *et al* (2021), one may dramatically reduce the execution time of a fluid model for magnetized plasma by fitting analytical functions to lookup tables produced from the electron rate and transport coefficients calculated by BOLSIG+.

In an alternative approach, however, it is possible to use the electron rate and transport coefficients corresponding to an effective electric field E_{eff} in non-magnetized plasma (i.e. $\vec{B}=0$) to deduce plasma transport parameters for the magnetized case (i.e. $\vec{B}\neq 0$). Compared to interpolating values from 3D lookup tables corresponding to $(E/N,\omega_{ce}/N,\angle\vec{E},\vec{B})$, the proposed method requires solving a transcendental equation to obtain E_{eff}, and subsequently using pre-computed rate and transport coefficient vectors to obtain values corresponding to E_{eff}/N. Based on the authors' experience, 3D interpolation in a high-resolution plasma fluid model is more time-consuming than solving a transcendental equation. The authors have not compared the efficiency of the transcendental method with calculations using analytical functions fitted to 3D lookup tables (e.g. Starikovskiy *et al* 2021). Overall, we emphasize that the calculations realized through the fitting functions, the lookup tables, or the proposed transcendental method do not represent the most computationally expensive parts of models (i.e. streamer models (Starikovskiy *et al* 2021, Janalizadeh and Pasko 2023)). In non-magnetized cases, we do not create lookup tables for different E and N values. Instead, we use the E/N-dependent (i.e. reduced) representations. The physics-based simplicity of the proposed formulation can be viewed as more efficient from the same perspective.

The majority of the present work is dedicated to the development of the theoretical background quantifying E_{eff}. Nevertheless, to accommodate readers interested mainly in the implementation aspect of the introduced method, in section 2 we describe the procedure to implement a simple and intuitive approximation to the general transcendental framework, which in later sections will be presented in detail. We conclude section 2 after demonstrating that the approximate method results in electron transport parameters in pure CO_2 plasma, that are in satisfactory agreement with BOLSIG+'s exact calculations for $\vec{B}\neq 0$.

Section 3 sets the theoretical foundation required for the introduction of the effective electric field E_{eff} mentioned above. Here it is demonstrated that E_{eff}, defined through the minimization of a designed error function, is in the same format of the electric field as an electron with energy ε (in electronvolts (eV)) experiences in the presence of a magnetic field (e.g. Starikovskiy *et al* 2021, equation (5)). Specifically, for a given magnitude of applied magnetic field (i.e. for specified ω_{ce}/N) and for a given angle between the electric field $\vec{E}$ and magnetic field $\vec{B}$ applied to a weakly ionized plasma, the influence of $\vec{B}$ on the ensemble of electrons may be interpreted in terms of an effective Hall parameter β_{eff}, which itself varies as a function of E_{eff}/N. Hereafter, we distinguish between the conventional energy-dependent Hall parameter $\beta_H(\varepsilon)=\omega_{ce}/\nu_m(\varepsilon)$ (where $\omega_{ce}=q_eB/m_e$, q_e is the fundamental charge of an electron, m_e is the mass of an electron, and $\nu_m(\varepsilon)$ is the effective momentum transfer collision frequency that is a function of ε) and β_{eff}, with the subscript 'H' used only for the former. Moreover, the dependence of quantities on the electron energy or velocity will be explicitly shown via a trailing '(ε)' or '(v)', respectively. That is, the absence of '(ε)' or '(v)' in the symbol of any plasma rate and transport coefficient implies that the corresponding coefficient has been averaged over the electron energy distribution function (EEDF). We note that the quantification of $\nu_m(\varepsilon)$ for collisions of electrons with each species in a mixture requires an effective electron impact cross-section, which as mentioned in the LXCat cross-section file accompanying BOLSIG+ (Hagelaar and Pitchford 2005), equals the sum of the elastic momentum transfer cross-section and total inelastic collision cross-section. This effective cross-section is not in any way connected to the concept of E_{eff} mentioned above.

The mathematical derivations related to section 3 may be found in appendix A, where the general transcendental method is derived. Here, we also discuss the weight function $w(v)$ (where $v=\gamma\varepsilon^{\frac{1}{2}}$ in which $\gamma=(2q_e/m_e)^{\frac{1}{2}}$) that is introduced in the definition of the error function mentioned

above. Subsequently, in section 4.1 it is demonstrated that three custom weight functions investigated as part of this analysis provide similar values for β_{eff}, and consequently we focus on one specific weight function, which results in the presented formulation lending itself to the electron rate and transport coefficients of magnetized plasma defined in e.g. Hagelaar (2016), and in some cases, directly outputted by BOLSIG+. This transition is explained in appendix B. In appendix C, further approximations justified in the case of nearly constant momentum transfer collision frequency as a function of the electron energy are introduced. This is where the simple and intuitive approximation to the general transcendental method, presented in section 2, is justified. In section 4.2 and through the comparison of some electron transport and rate coefficients with BOLSIG+ calculations corresponding to $\vec{B} \neq 0$, it is demonstrated that the proposed transcendental method, in exact and approximate form, and the magnetized plasma (i.e. $\vec{B} \neq 0$) calculations of BOLSIG+ give consistent results. The limit of nearly constant $\nu_{\text{m}}(\varepsilon)$ is also discussed. The validity of the presented transcendental framework is demonstrated through application to three gas mixtures, i.e. air, a mixture of 88% molecular hydrogen with 12% helium representing the composition of giant gaseous planets in the Solar System, and pure carbon dioxide.

2. Model outline

The electron transport and rate coefficients in various gas mixtures for the non-magnetized (i.e. $\vec{B} = 0$) case are commonly represented as functions of the reduced applied field E/N using lookup tables or various fits with analytical functions. These are usually formulated using a combination of the solution of kinetic equations, swarm experiments, and Monte Carlo simulations, and are readily available to modelers. An example of these would be solutions corresponding to $\vec{B} = 0$ in CO_2 gas recently published in Starikovskiy *et al* (2021). The purpose of this section is to demonstrate that these $\vec{B} = 0$ representations can be directly used to obtain transport and rate coefficients for an arbitrary magnitude and direction of the applied magnetic field $\vec{B} \neq 0$. We note that ideas of self-consistently accounting for the electron momentum transfer collision frequency varying as a function of the applied electric field in the evaluation of the electron conductivity tensor in weakly ionized plasmas have appeared in previous publications (Pasko *et al* 1998, Marshall 2009, Marshall *et al* 2010, Kabirzadeh *et al* 2015, Salem *et al* 2016, Tonev and Velinov 2016). However, these approaches have not been rigorously justified.

While a rigorous formulation and discussion of the validity of the proposed transcendental method follows in the subsequent sections, here we focus on the implementation of an approximation to the general transcendental method to illustrate and emphasize the accuracy and efficiency of the transcendental method in its simplest form (see appendix C). We note that in this case, the effective electric field E_{eff} in the presence of a magnetic field is given by the proposed method via

$$E_{\text{eff}}^2 = E_{\parallel}^2 + \frac{E_{\perp}^2}{1+\beta_{\text{eff}}^2(E_{\text{eff}})} = E_{\parallel}^2 + \frac{E_{\perp}^2}{1+(\omega_{\text{ce}}/\nu_{\text{m}})^2} \quad (1)$$

which resembles the expression of the electric field that an electron with energy ε experiences due to the presence of a magnetic field (e.g. Starikovskiy *et al* 2021, equation (5)). Whereas the Hall parameter $\beta_{\text{H}}(\varepsilon) = \omega_{\text{ce}}/\nu_{\text{m}}(\varepsilon)$ (e.g. Starikovskiy *et al* 2021, equation (5)), where $\nu_{\text{m}}(\varepsilon)/N$ is the rate constant for momentum transfer due to an electron with energy ε, in equation (1) $\beta_{\text{eff}} = \omega_{\text{ce}}/\nu_{\text{m}}$, where $\nu_{\text{m}}/N = k_{\text{m}}(E_{\text{eff}}/N)$ is the rate constant for momentum transfer (averaged over the EEDF). This implies that, expressed explicitly, $\beta_{\text{eff}} = \beta_{\text{eff}}(E_{\text{eff}}/N, \omega_{\text{ce}}/N)$. Nevertheless, in equation (1) the dependence of β_{eff} on ω_{ce}/N is suppressed, assuming that analysis is conducted for a constant applied magnetic field providing a constant value of ω_{ce}/N. Also, the dependence of β_{eff} on E_{eff}/N is denoted solely by E_{eff} to make a connection to the fixed point x of a function $\phi(x)$ defined as $x = \phi(x)$, where in equation (1) $x = E_{\text{eff}}$ and thus, $\phi(x) = \left[E_{\parallel}^2 + \frac{E_{\perp}^2}{1+\beta_{\text{eff}}^2(x)}\right]^{\frac{1}{2}}$. The concept of a fixed point in addition to the fixed-point theorem is invoked in appendix E and the supplementary file to discuss the existence, uniqueness, and convergence of a solution E_{eff} to non-linear equation (1).

For a given $(E/N, \omega_{\text{ce}}/N, \angle\vec{E}, \vec{B})$, such that $E_{\parallel} = E\cos(\angle\vec{E}, \vec{B})$ and $E_{\perp} = E\sin(\angle\vec{E}, \vec{B})$ are the components of the applied electric field $\vec{E}$, respectively, parallel and perpendicular to the magnetic field $\vec{B}$, the approximate transcendental method only requires ν_{m}/N, which is related to the electron mobility μ_{e} via $\nu_{\text{m}}/N = (\gamma^2/2)/(\mu_{\text{e}}N)$ (i.e. $\nu_{\text{m}} = q_{\text{e}}/(m_{\text{e}}\mu_{\text{e}})$ in the absence of Coulomb collisions) (Hagelaar 2016, p 17). We emphasize that this formulation employs only ν_{m}/N (or equivalently, β_{eff} in equation (1)) as a function of the reduced effective electric field E_{eff}/N, i.e. ν_{m}/N is a function of E_{eff}/N only, and is calculated with no effect of the applied magnetic field, i.e. $\vec{B} = 0$. In practice, μ_{e} can be interpreted as mobility parallel to the magnetic field $\mu_{\parallel}$. Furthermore, β_{eff} introduced here is an approximation to the β_{eff} quantity defined in section 3.

There are a number of sources available that may be used to calculate the electron mobility in various gas mixtures for the $\vec{B} = 0$ case. For instance, in addition to the electron mobility in air, Morrow and Lowke (1997) provide analytic functions for electron impact collision rate constants, which were used in previous modelings of streamers in air (e.g. Bourdon *et al* 2007, Jánský and Pasko 2020). Additionally, Moss *et al* (2006) provided a MATLAB function `air1.m` compiled from the results of ELENDIF (Morgan and Penetrante 1990), which returns electron mobility and mean energy in addition to rate coefficients for various electron impact processes in air. This function is freely available at http://pasko.ee.psu.edu/air. There are similar MATLAB functions based on

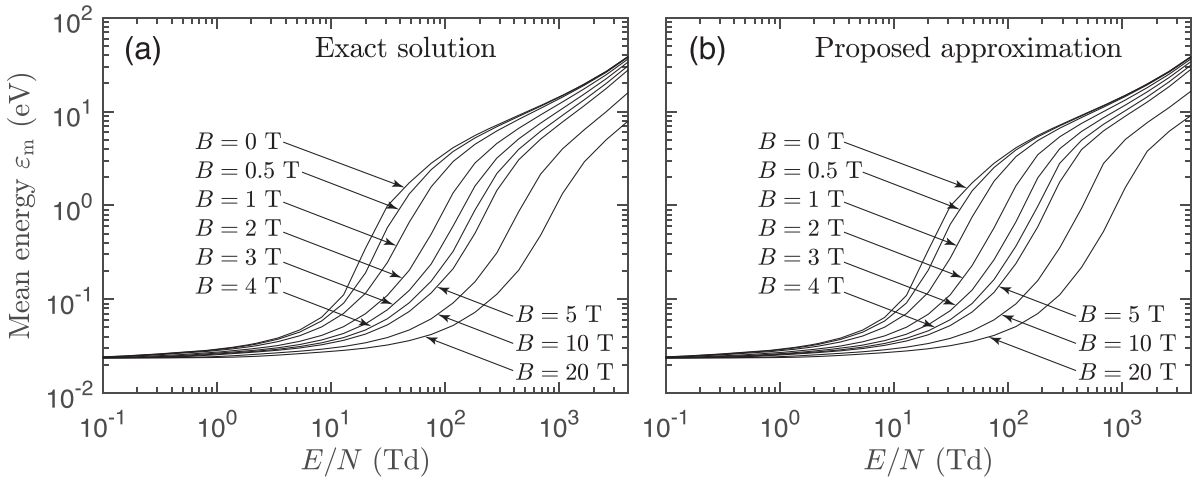

Figure 1. Electron mean energy as a function of the applied reduced electric field E/N calculated using (a) BOLSIG+, and (b) the approximate transcendental method for various values of the magnetic field B in pure CO_2 when $\vec{E} \perp \vec{B}$. Panel (a) is an independent reproduction of Starikovskiy *et al* (2021), figure 4(a), where $N = 1.6447 \times 10^{24}$ m^{-3} corresponds to pressure $p = 50$ Torr and temperature $T = 293$ K. Note that as mentioned in Starikovskiy *et al* (2021), $E/N = 1\,\text{Td} = 10^{-17}$ V cm^2 corresponds to $E = 25$ kV m^{-1} for $p = 1$ atm and $T = 293$ K.

BOLSIG+ (Hagelaar and Pitchford 2005) for air (Janalizadeh and Pasko 2020), Jupiter's atmosphere (Janalizadeh and Pasko 2023), and CO_2 (provided per request from the authors).

Equation (1) is a transcendental equation for E_{eff} and may be solved for E_{eff} using electron mobility given by the functions mentioned above to quantify β_{eff}. Once the value of E_{eff} that satisfies equation (1) is obtained, the kinetics of electrons under the influence of $(E/N, \omega_{\text{ce}}/N, \angle\vec{E},\vec{B})$ are converted to an equivalent problem with $(E_{\text{eff}}/N, \vec{B} = 0)$. The electron rate and transport coefficients may then be calculated using the functions above, which were developed for non-magnetized plasma. In particular, the perpendicular and Hall mobilities may be obtained via $\mu_\perp = \mu_\parallel/(1+\beta_{\text{eff}}^2)$ and $\mu_{\text{H}} = \mu_\times = \mu_\parallel \beta_{\text{eff}}/(1+\beta_{\text{eff}}^2)$, respectively.

Figure 1(a) depicts the mean energy of electrons ε_{m} in CO_2 gas under the influence of external electric and magnetic fields obtained using BOLSIG+ with accurate inclusion of an external magnetic field, while figure 1(b) depicts the same results calculated using the proposed transcendental method (i.e. equation (1)). It may be inferred that the approximate transcendental method provides results in satisfactory agreement with BOLSIG+'s exact calculations. We note that figure 1(a) is a reproduction of Starikovskiy *et al* (2021), figure 4(a), where the authors also use BOLSIG+ to calculate the electron mean energy. Here, we do not present the results corresponding to Starikovskiy *et al* (2021), figures 4(b)–(d), since in that study the respective ionization frequency ν_{i}, electron mobility parallel to the magnetic field vector $\mu_\parallel$, and electron mobility perpendicular to the magnetic field vector $\mu_\perp$ are presented as dimensionless quantities. Instead, in figure 2, we compare the results of BOLSIG+ and the transcendental method for ε_{m}, ν_{i}, $\mu_\parallel$, and $\mu_\perp$, as a function of $\angle\vec{E},\vec{B}$. Here, the applied electric field $E = 1.5E_k$, where $E_k \simeq 80$ Td (1 Td $= 10^{-17}$ V cm^2) is the breakdown electric field (Raizer 1991, p 137) in pure CO_2 calculated via BOLSIG+. The values of the reduced electron cyclotron frequency used for the calculations are $(\omega_{\text{ce}}/N)_1 = 10^{-14}$, $(\omega_{\text{ce}}/N)_2 = 10^{-13}$, and $(\omega_{\text{ce}}/N)_3 = 10^{-12}$ rad m^3 s^{-1}. As seen later in section 4.1, this interval of ω_{ce}/N covers the entire range between non-magnetized ($\beta_{\text{eff}}^2 \ll 1$) and highly magnetized ($\beta_{\text{eff}}^2 \gg 1$) electrons, and consequently it is demonstrated in figure 2 that the results from the two methods are in satisfactory agreement in the entire range of magnetized CO_2 plasma. In particular, as demonstrated in equation (A.15), the error of the transcendental method grows approximately proportional to $\sin^4(\angle\vec{E},\vec{B})$. Thus, the maximum discrepancy between the exact and transcendental results occurs at $\angle\vec{E},\vec{B} = 90°$. Furthermore, for non-magnetized (fully magnetized) plasma both the exact and transcendental method trivially return $E_{\text{eff}} = E$ ($E_{\text{eff}} = E_\parallel$). This agreement between the two methods does not necessarily hold for partially magnetized plasma, where $\beta_{\text{eff}} \gtrsim 1$.

Before ending this section, we reiterate the outline used above for studies that require calculation of the electron rate and transport coefficients in a magnetized plasma. As demonstrated above, this approach reduces the problem of magnetized plasma (i.e. $\vec{B} \neq 0$) in the presence of an applied electric field $\vec{E}$ to an equivalent problem of non-magnetized plasma (i.e. $\vec{B} = 0$) in the presence of an effective electric field E_{eff} where one

1. Calculates E_{eff} for a given $(E/N, \omega_{\text{ce}}/N, \angle\vec{E},\vec{B})$ satisfying the transcendental equation (1), and corresponding $\beta_{\text{eff}}(E_{\text{eff}}/N)$.
2. Calculates electron transport and rate coefficients as if $\vec{B} = 0$ using this newly obtained E_{eff}. For instance, electron mean energy $\varepsilon_{\text{m}}(E_{\text{eff}}/N)$, reduced electron impact ionization frequency $\frac{\nu_{\text{i}}}{N}(E_{\text{eff}}/N)$, reduced momentum

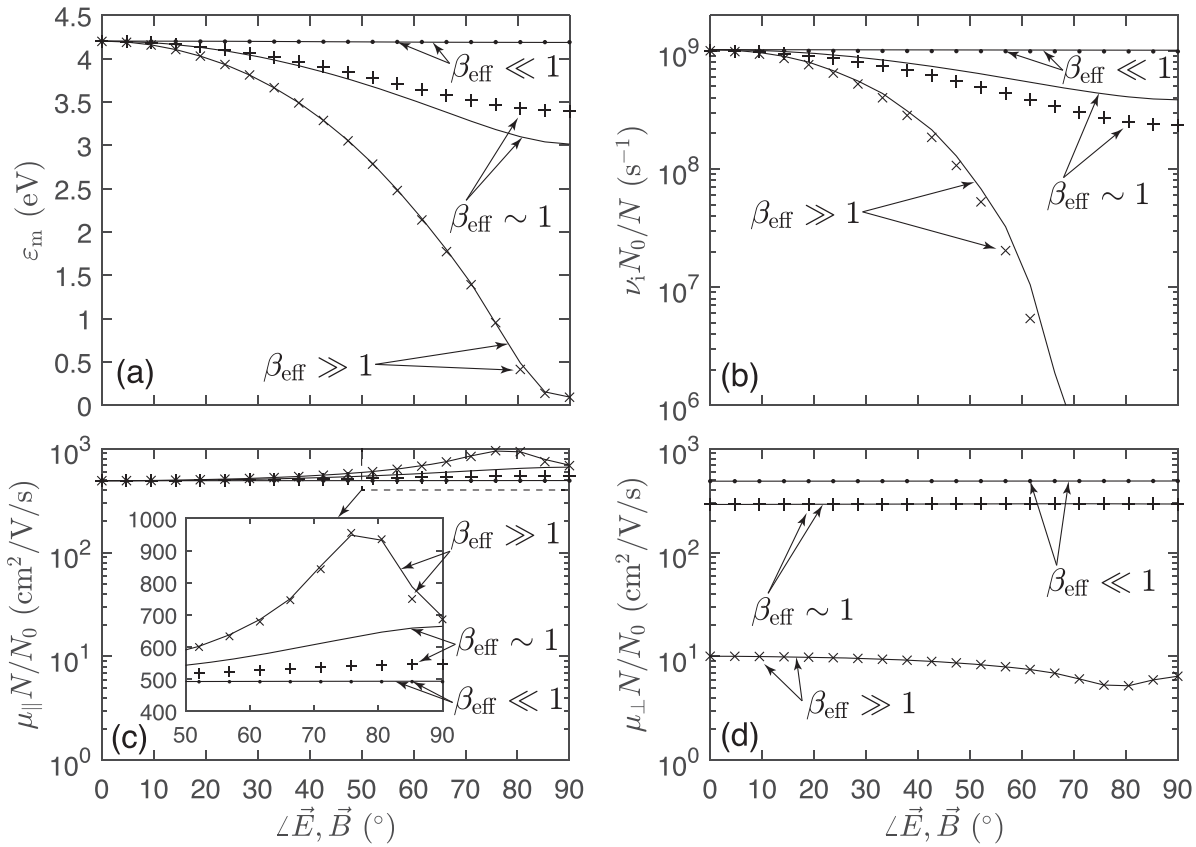

Figure 2. (a) Electron mean energy, (b) reduced electron-impact ionization frequency $\nu_i N_0/N$, (c) reduced electron mobility parallel to magnetic field $\mu_\parallel N/N_0$, and (d) reduced electron mobility perpendicular to magnetic field $\mu_\perp N/N_0$ as a function of the angle between the electric field $E = 1.5E_k$ ($E_k = 80$ Td) and the magnetic field calculated for $(\omega_{ce}/N)_1 = 10^{-14}$ rad m^3 s^{-1} (•), $(\omega_{ce}/N)_2 = 10^{-13}$ rad m^3 s^{-1} (+), and $(\omega_{ce}/N)_3 = 10^{-12}$ rad m^3 s^{-1} (×) in pure CO_2 gas. Solid lines denote BOLSIG+ exact calculations and markers denote the approximate transcendental method. The Loschmidt number $N_0 = 2.686 \times 10^{25}$ m^{-3}. See figure 3(c) for numerical values of β_{eff} corresponding to $(\omega_{ce}/N)_{1-3}$ used here.

transfer collision frequency $\frac{\nu_m}{N}(E_{eff}/N)$, reduced electron mobility parallel to the magnetic field $\mu_\parallel N = (q_e/m_e)/\left(\frac{\nu_m}{N}(E_{eff}/N)\right)$, and electron mobility perpendicular to the magnetic field $\mu_\perp = \mu_\parallel/\left(1+\beta^2_{eff}(E_{eff}/N)\right)$.

The solution of equation (1) can be simplified if, for a given ω_{ce}/N, $\beta_{eff} = (\omega_{ce}/N)/(\nu_m/N)$ can be assumed to be constant or weakly dependent on the reduced electric field E_{eff}/N. However, we note that for typical electric fields used in applications, the β_{eff} parameter in equation (1) can exhibit significant variations as a function of E_{eff}/N. For example, for CO_2 gas, it changes by a factor of 5, and for air by a factor of 10. As β_{eff} enters equation (1) in a quadratic form, these variations are important and one needs to find the solution E_{eff} of nonlinear equation (1) to accurately solve the problem. The solutions can be simplified when $\beta^2_{eff} \ll 1$ due to the high collision frequency $\nu_m(E_{eff}/N;N) \gtrsim \omega_{ce}$ in strong applied electric fields (e.g. Liu *et al* 2017) or when the orientation of the electric field with respect to the magnetic field has preferentially an $E_\parallel$ component (e.g. Pérez-Invernón *et al* 2018). In both cases, the effect of an external magnetic field on the system behavior can be ignored. We note that the solution flow described here follows from the case labeled as $w = w_3$ for $\beta^2_H(\varepsilon) \gg 1$, where w is a weight function that will be defined in the following section.

3. Model formulation

Assuming a steady state and homogeneous space, in the presence of a constant electric and magnetic field, the isotropic part of the electron velocity distribution function (EVDF) f_{0_B} in the Lorentzian approximation (e.g. Holstein 1946) $f_B(\vec{v}) = f_{0_B}(v) + \vec{f}_{1_B}(v)\cdot\vec{i}_v$, where $\vec{i}_v$ is the radial unit vector in velocity space, is the solution to the differential equation (e.g. Golant *et al* 1980, p 140)

$$\frac{1}{3}\left(\frac{q_e}{m_e}\right)^2 \frac{1}{v^2}\frac{\partial}{\partial v}\left[\frac{v^2}{\nu_m(v)}\left(\frac{E^2_\perp}{1+\beta^2_H(v)} + E^2_\parallel\right)\frac{\partial f_{0_B}}{\partial v}\right] + C(f_{0_B}) = 0 \tag{2}$$

where the subscript B emphasizes that the EVDF is calculated for magnetic field $\vec{B} \neq 0$. The anisotropic part $\vec{f}_{1_B}$ is given in

e.g. Loureiro and Amorim (2016, p 164) for $\vec{B} \parallel \hat{z}$, where $\hat{z}$ is a unit vector in the direction of the z axis. In the above equation and in a conventional cylindrical coordinate system, we have $E_\perp^2 = E_\rho^2 + E_\varphi^2, E_\parallel = E_z$, $E^2 = E_\perp^2 + E_\parallel^2$, and $\beta_{\rm H}(\varepsilon) = \omega_{\rm ce}\nu_{\rm m}^{-1}(\varepsilon)$. Also, $\angle\vec{E},\vec{B}$ is the angle between $\vec{E}$ and $\vec{B}$ such that $\tan(\angle\vec{E},\vec{B}) = \frac{E_\perp}{E_\parallel}$, and $C(f_{0_B})$ denotes the collision term (e.g. Loureiro and Amorim 2016, pp 101–4, 110–5). The solution of equation (2) as a function of v varies with any combination of $(E/N, \omega_{\rm ce}/N, \angle\vec{E},\vec{B})$, i.e. $f_{0_B} = f_{0_B}(v; E/N, \omega_{\rm ce}/N, \angle\vec{E},\vec{B})$ (e.g. Janalizadeh and Pasko 2023, appendix A2). For the remainder of this work, symbols after a semicolon represent independent external parameters on which an introduced quantity depends.

As a result of the Lorentzian, i.e. two-term expansion of the EVDF, electron impact collision rates are determined exclusively by f_{0_B} ($\int_{v=0}^{\infty} f_{0_B}(v) 4\pi v^2 {\rm d}v = n_{\rm e}$, where $n_{\rm e}$ denotes electron density). On the other hand, electron transport coefficients are dependent on $\vec{f}_{1_B}$. As can be seen from sources cited above (e.g. Janalizadeh and Pasko 2023, appendix A1), for a given set of $(E/N, \omega_{\rm ce}/N, \angle\vec{E},\vec{B})$, the latter is solely dependent on the derivative of the isotropic term with respect to v. Thus, in an alternative approach that does not require solving equation (2) for magnetized electrons, here we substitute f_{0_B} with f_0 in search of the isotropic part of an EVDF in the absence of a magnetic field, i.e. $\vec{B} = 0$, that minimizes the residual

$$R(v) = R[f_0(v)] = \frac{1}{3}\left(\frac{q_{\rm e}}{m_{\rm e}}\right)^2 \frac{1}{v^2}\frac{\partial}{\partial v}\left[\frac{v^2}{\nu_{\rm m}(v)}\left(\frac{E_\perp^2}{1+\beta_{\rm H}^2(v)} + E_\parallel^2\right)\frac{\partial f_0}{\partial v}\right] + C(f_0) \tag{3}$$

over the $v \in [0,\infty]$ interval. Before presenting the minimization process, we note that, as demonstrated in equation (2), the residual is zero for f_{0_B}. As such, $R(v)$ may be interpreted as a measure quantifying the difference between f_{0_B} and $f_0 = f_0(v; E_{\rm eff}/N)$ at a given electron velocity v. We note that $f_0(v)$ is the solution to (e.g. Raizer 1991, p 87)

$$\frac{1}{3}\left(\frac{q_{\rm e}}{m_{\rm e}}\right)^2 \frac{1}{v^2}\frac{\partial}{\partial v}\left[\frac{v^2}{\nu_{\rm m}(v)} E_{\rm eff}^2 \frac{\partial f_0}{\partial v}\right] + C(f_0) = 0 \tag{4}$$

where we have let $\beta_{\rm H}(v) = 0$ in equation (2) to obtain the above equation for a given $E_{\rm eff}$. Subsequently, we can replace the collision term $C(f_0)$ in equation (3) using the definition in equation (4) to obtain

$$R(v) = \frac{1}{3}\left(\frac{q_{\rm e}}{m_{\rm e}}\right)^2 \frac{1}{v^2}\frac{\partial}{\partial v}\left[\frac{v^2}{\nu_{\rm m}(v)}\left(\frac{E_\perp^2}{1+\beta_{\rm H}^2(v)} + E_\parallel^2 - E_{\rm eff}^2\right)\frac{\partial f_0}{\partial v}\right]. \tag{5}$$

Note that $R(v)$ expressed in equation (5) resembles the signed difference between the increase per unit volume of velocity space per unit time of electron density due to the presence of $\vec{E}$ and $\vec{B}$ versus the presence of $E_{\rm eff}$ (when $\vec{B} = 0$) (e.g. Loureiro and Amorim 2016, p 105).

The minimization of the defined residual over $v \in [0,\infty]$ may be quantified by introducing a weight function $w(v)$ and subsequently defining an error function

$$\mathcal{E}(E_{\rm eff}/N; E/N, \omega_{\rm ce}/N, \angle\vec{E},\vec{B}) = \|R\|^2 = \langle R, R\rangle = \int_{v=0}^{\infty} R^2(v) w(v) {\rm d}v \tag{6}$$

where we have used the definition of the inner product $\langle f, g\rangle = \int_{v=0}^{\infty} f^*(v) g(v) w(v) {\rm d}v$ (e.g. Dudley 1994, p 53), in which * represents the complex conjugate operator. Here, we wish to find the value of $E_{\rm eff}$ that minimizes the error $\mathcal{E}$. By definition, in that case we should have $\partial\mathcal{E}/\partial E_{\rm eff} = 0$. We emphasize that this minimization should generally be performed for every set of three independent external parameters used in the formulation of lookup tables (e.g. Starikovskiy *et al* 2021), namely, E/N, $\omega_{\rm ce}/N$, and $\angle\vec{E},\vec{B}$. Nevertheless, as demonstrated in appendix A, this analysis results in the general transcendental expression

$$E_{\rm eff}^2 = E_\parallel^2 + \frac{E_\perp^2}{1+\beta_{\rm eff}^2} \tag{7}$$

where $\sqrt{1+\beta_{\rm eff}^2}$ is the factor by which the perpendicular component of the applied electric field is reduced due to the presence of a magnetic field. The quantity $\beta_{\rm eff}$ varies only as a function of $E_{\rm eff}/N$ for a given $\omega_{\rm ce}/N$ and is given by $\beta_{\rm eff} = \sqrt{I_1/I_2 - 1}$, where I_1 and I_2 are integrals defined in equations (A.6) and (A.7), respectively. The dependence of $\beta_{\rm eff}$ (through I_2) on $\omega_{\rm ce}/N$ is only through $\beta_{\rm H}(\varepsilon)$ since as already mentioned, f_0 corresponds to a non-magnetized EVDF such that one does not need to solve equation (2) for magnetized plasma.

Generally, $E_{\rm eff}$ will be located in the $[E\cos(\angle\vec{E},\vec{B}), E]$ interval where the upper (lower) limit of this search interval corresponds to non-magnetized, $\beta_{\rm eff}^2 \ll 1$, (fully magnetized, $\beta_{\rm eff}^2 \gg 1$) electrons, respectively. Therefore, once $\beta_{\rm eff}$ is quantified, one can employ a root-finding algorithm to solve equation (7) and obtain $E_{\rm eff}/N$ for a given set of input parameters $(E/N, \omega_{\rm ce}/N, \angle\vec{E},\vec{B})$. The question of the existence and uniqueness of a solution to equation (7) is addressed in appendix E. Specifically, it is demonstrated that a solution always exists, and conditions for the uniqueness of a solution and convergence of the fixed-point iteration method to find $E_{\rm eff}$ are obtained such that for any given set of input parameters $(E/N, \omega_{\rm ce}/N, \angle\vec{E},\vec{B})$ one can verify these conditions. We note that the interested reader may accelerate the root-finding process by creating a two-dimensional array of $\beta_{\rm eff}$ values varying as a function of the $(E_{\rm eff}/N, \omega_{\rm ce}/N)$ pair to be subsequently used in solving the transcendental equation (7).

To numerically quantify $\beta_{\rm eff}$ we introduce three weight functions denoted by $w_1(v), w_2(v), w_3(v)$ to demonstrate the performance of the presented transcendental method. The corresponding weight function in energy space is defined via $W(\varepsilon){\rm d}\varepsilon \equiv w(v){\rm d}v$, where, as mentioned above, ε denotes electron energy in units of eV. The weight functions we use in this work are

1. $w_1(v) = 1$, i.e. constant weight function in velocity space. Thus, $W(\varepsilon) = \frac{\gamma}{2}\varepsilon^{-\frac{1}{2}}$
2. $w_2(v) = \frac{1}{n_e} f_0(v) 4\pi v^2$ such that $w_2(v)\mathrm{d}v = \frac{1}{n_e}\frac{n_e}{2\pi\gamma^3} F_0(\varepsilon) 4\pi\gamma^2 \varepsilon \frac{\gamma}{2}\varepsilon^{-\frac{1}{2}}\mathrm{d}\varepsilon = P_0(\varepsilon)\mathrm{d}\varepsilon$
3. $w_3(v) = v^6\left[\frac{\partial}{\partial v}\left(\frac{v^2}{\nu_m(v)}\frac{\partial f_0}{\partial v}\right)\right]^{-1}$ such that

$$w_3(v)\mathrm{d}v = \frac{\left(\gamma^2\varepsilon\right)^3}{2\gamma^{-1}\varepsilon^{\frac{1}{2}}\frac{\partial}{\partial\varepsilon}\left\{\frac{\gamma^2\varepsilon}{\nu_m(\varepsilon)}2\gamma^{-1}\varepsilon^{\frac{1}{2}}\frac{\partial}{\partial\varepsilon}\left[\frac{n_e}{2\pi\gamma^3}F_0(\varepsilon)\right]\right\}}\frac{\gamma}{2}\varepsilon^{-\frac{1}{2}} \times \mathrm{d}\varepsilon = \frac{\pi\gamma^{10}}{4n_e}\frac{\varepsilon^2\mathrm{d}\varepsilon}{\frac{\partial}{\partial\varepsilon}\left[\frac{\varepsilon^{\frac{3}{2}}}{\nu_m(\varepsilon)}\frac{\partial F_0}{\partial\varepsilon}\right]} \tag{8}$$

where the EEDF in BOLSIG+ $F_0(\varepsilon)$ and the electron probability distribution function (EPDF) $P_0(\varepsilon)$ are defined in appendix D. Note that since $\beta_{\mathrm{eff}} \propto I_1/I_2$, the absolute value of the electron density or the constant γ present in the weight function do not affect any results of this analysis as the weight function is included in both I_1 and I_2.

We emphasize that the formulation presented here is valid irrespective of the peculiarities of each weight function. As such, in choosing w_1 and w_2 we prioritize the simplicity of the weight function itself. However, this is not the case for w_3. Specifically, w_3 has been chosen such that β_{eff} will become proportional to the electron transport and rate coefficients directly outputted by BOLSIG+ (see appendices B and C). In other words, calculating β_{eff} when $w = w_1$ or $w = w_2$ requires the EEDF calculated by BOLSIG+ for evaluation of the integrals I_1 and I_2. However, when $w = w_3$ these integrals reduce to specific electron rate and transport coefficients that are already calculated by BOLSIG+ in the non-magnetized case (i.e. $\vec{B} = 0$).

Specifically, the transcendental method in the special case of $w = w_3$ reduces to (see appendix B)

$$E_{\mathrm{eff}}^2 = E_{\parallel}^2 + \frac{E_{\perp}^2}{\left(\frac{\mu_{\parallel}}{\mu_{\perp}^0}\right)} \tag{9}$$

where expressions for mobilities parallel $\mu_{\parallel}$ and perpendicular $\mu_{\perp}$ to the magnetic field are given in equations (B.5) and (B.9), respectively (e.g. Hagelaar 2016, p 16). We note that whereas $\mu_{\perp}^0$ is in the same format of $\mu_{\perp}$ defined in Hagelaar 2016, p 16, as opposed to $\mu_{\perp}$ it is not a direct output of BOLSIG+ since the calculation of $\mu_{\perp}$ by BOLSIG+ happens when $\vec{B} \neq 0$, while $\mu_{\perp}^0$ is dependent on BOLSIG+ only through BOLSIG+'s EEDF calculated for $\vec{B} = 0$. As such, we calculate $\mu_{\perp}^0$ manually (in MATLAB) using the EEDF output of BOLSIG+ corresponding to a defined range of E_{eff}/N values. A given reduced gyrofrequency ω_{ce}/N quantifies $\beta_H(\varepsilon) = \omega_{ce}/\nu_m(\varepsilon)$ in the definition of $\mu_{\perp}^0$ through $\nu_m(\varepsilon) = N\sigma_m(\varepsilon)v = N\sigma_m(\varepsilon)\gamma\varepsilon^{\frac{1}{2}}$. In the calculation of $\mu_{\perp}^0$ and more generally β_{eff}, we quantified the momentum transfer cross-section $\sigma_m(\varepsilon)$ of each gas mixture using the LXCat set of cross-sections, which accompanied BOLSIG+. For species for which $\sigma_m(\varepsilon)$ was not readily available in the accompanying data, we calculated $\sigma_m(\varepsilon)$ by summing the cross-section for all inelastic processes in addition to the elastic momentum transfer cross-section. The value of $\sigma_m(\varepsilon)$ for a mixture was obtained by weighted summation of $\sigma_m(\varepsilon)$ of the constituent species according to their fraction of composition.

4. Results and discussion

4.1. Calculation of β_{eff} for $w_1(v), w_2(v)$, and $w_3(v)$

As inferred from section 3, whereas the determination of E_{eff} through the transcendental equation is dependent on the applied electric and magnetic fields in addition to the angle between the two, the calculation of β_{eff} for a given E_{eff}/N may proceed in a standalone fashion. To quantify β_{eff} for various weight functions, here we use BOLSIG+ to calculate the EEDF (with $\vec{B} = 0$) in gas mixtures considered for a wide range of E_{eff}/N values. As already mentioned, the magnetic field enters our calculations of β_{eff} only through the Hall parameter included in the definition of I_2. Three gas mixtures are considered: (1) air, i.e. a mixture of 80% molecular nitrogen (N_2) and 20% molecular oxygen (O_2), (2) a mixture of 88% molecular hydrogen (H_2) and 12% helium (He), and (3) pure carbon dioxide (CO_2).

In figure 3 we illustrate the calculated values of β_{eff}. We note that the reduced breakdown electric fields (e.g. Raizer 1991, p 137) in mixtures (1)–(3) have been calculated via BOLSIG+ and are respectively ∼120, 40, and 80 Td. In air and pure CO_2 we choose $E_{\mathrm{eff}}/N = 10^0 - 10^3$ Td. Due to the much lower breakdown threshold in mixture (2), results are shown for a maximum of $E_{\mathrm{eff}}/N = 500$ Td. The values of the reduced gyrofrequency chosen for the calculations are $10^{-14}, 10^{-13}$, and 10^{-12} rad m^3 s^{-1}, and are respectively denoted by $(\omega_{ce}/N)_1, (\omega_{ce}/N)_2$, and $(\omega_{ce}/N)_3$. As seen in figure 3, this interval of ω_{ce}/N covers the entire range between non-magnetized ($\beta_{\mathrm{eff}}^2 \ll 1$) and highly magnetized ($\beta_{\mathrm{eff}}^2 \gg 1$) electrons. We note that in Starikovskiy *et al* (2021), magnetized streamers were studied in the $\omega_{ce}/N = 0 - 20 \times 10^{-13}$ rad m^3 s^{-1} range. Janalizadeh and Pasko (2023) modeled magnetized sprite streamers at 250 km altitude in the atmosphere of Jupiter, where $\omega_{ce}/N \simeq 1.4 \times 10^{-13}$ rad m^3 s^{-1}, and the reduced gyrofrequency at ∼100 km altitude in the atmosphere of Earth (where a lightning-induced transient luminous event referred to as an elve was observed (e.g. Fukunishi *et al* 1996) and further modeled (e.g. Marshall *et al* 2010)) is $\omega_{ce}/N \simeq 5.8 \times 10^{-13}$ rad m^3 s^{-1}.

Furthermore, it is inferred from figure 3 that the difference between β_{eff} values corresponding to various weight functions $w(v)$ is practically insignificant. As already mentioned in section 3, $w = w_3$ results in the expression of β_{eff} in terms of the electron rate and transport coefficients, which are already calculated by BOLSIG+ in the non-magnetized case (i.e. $\vec{B} = 0$). Therefore, for the sake of simplicity and brevity, in the remainder of this work we let $w = w_3$.

4.2. Comparison of BOLSIG+ exact coefficients with present study results

As demonstrated in appendix C, when $w = w_3$, the presented transcendental method for considerably magnetized electrons may be simplified even further. Specifically, if $\langle\varepsilon\frac{\partial}{\partial\varepsilon}[\sigma_m(\varepsilon)\varepsilon^{\frac{1}{2}}]\rangle \equiv \int_{\varepsilon=0}^{\infty}\varepsilon\frac{\partial}{\partial\varepsilon}[\sigma_m(\varepsilon)\varepsilon^{\frac{1}{2}}]P_0(\varepsilon)\mathrm{d}\varepsilon$ is negligible, one

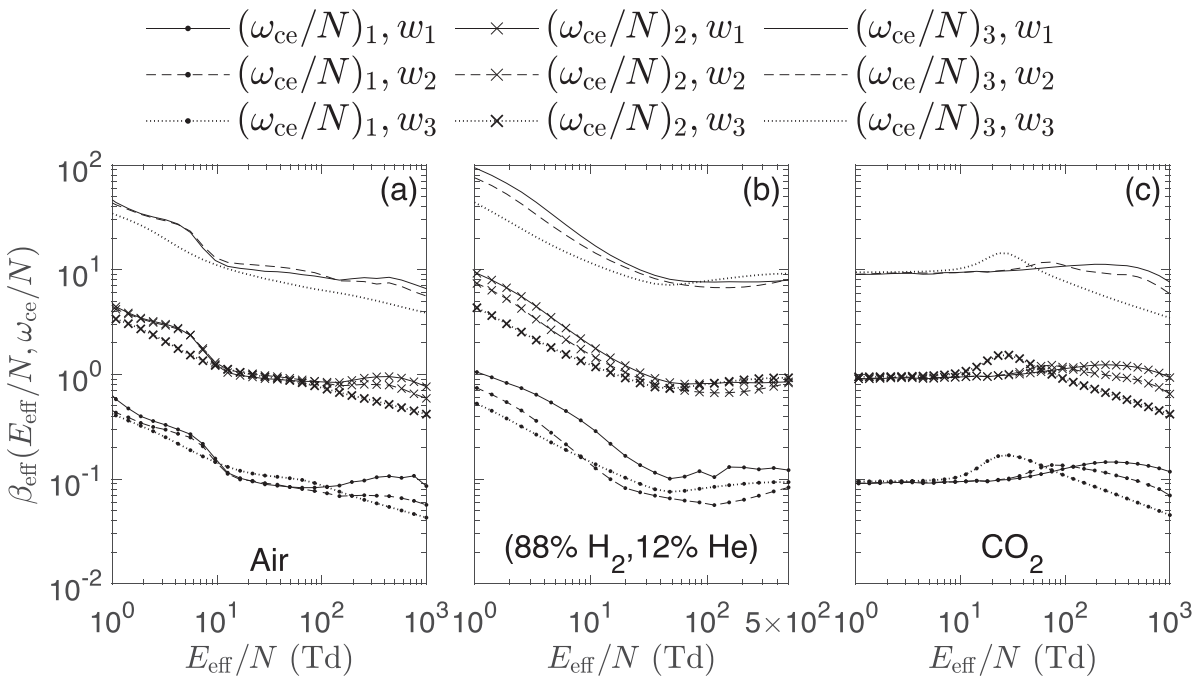

Figure 3. Values of $\beta_{\rm eff} = \beta_{\rm eff}(E_{\rm eff}/N; \omega_{\rm ce}/N)$ in (a) air, (b) 88% H_2, 12% He, and (c) pure CO_2 as a function of given reduced effective field $E_{\rm eff}/N$ for values of $(\omega_{\rm ce}/N)_1 = 10^{-14}$ rad m^3 s^{-1}, $(\omega_{\rm ce}/N)_2 = 10^{-13}$ rad m^3 s^{-1}, and $(\omega_{\rm ce}/N)_3 = 10^{-12}$ rad m^3 s^{-1}.

can use $\beta_{\rm eff} = \omega_{\rm ce}/\nu_{\rm m} = (\omega_{\rm ce}/N)/k_{\rm m}(E_{\rm eff}/N)$, where $k_{\rm m} = \nu_{\rm m}/N$ is the momentum transfer rate constant as a function of $E_{\rm eff}/N$ exclusively. This is a standard rate coefficient calculated by BOLSIG+ itself such that the implementation of the transcendental method using the EEDFs calculated by BOLSIG+ may be avoided. The average $\langle \varepsilon \frac{\partial}{\partial \varepsilon}[\sigma_{\rm m}(\varepsilon)\varepsilon^{\frac{1}{2}}]\rangle$ is a measure of the variation of momentum transfer collision frequency as a function of the electron energy. That is, $\sigma_{\rm m}(\varepsilon) \propto \varepsilon^{-\frac{1}{2}}$ for which the average is identically zero corresponds to a constant momentum transfer collision frequency since in that case $\nu_{\rm m}(\varepsilon) = Nk_{\rm m}(\varepsilon) = N\sigma_{\rm m}(\varepsilon)v \propto \varepsilon^{-\frac{1}{2}}(\gamma\varepsilon^{\frac{1}{2}}) = {\rm const}$ (e.g. Starikovskiy *et al* 2021). Consequently, in this section, we assume that this average is in fact negligible, and compare results with the general transcendental method with $w = w_3$ and $\beta_{\rm eff}$. We will also include the exact (no assumptions made) calculations of BOLSIG+, which have been compiled in lookup tables and subsequently interpolated for cases considered here.

Specifically, we consider two cases of $\angle\vec{E},\vec{B}$: 45° and 90° in addition to a large range of applied reduced fields E/N. We choose $\omega_{\rm ce}/N$ (or equivalently $\omega_{\rm ce}N_0/N$, where $N_0 = 2.686 \times 10^{25}$ m^{-3}) such that $\beta_{\rm eff} \simeq 1$ for both $\angle\vec{E},\vec{B}$ considered and in the majority of the E/N range. The purpose of this choice of $\omega_{\rm ce}N_0/N$ is to demonstrate the performance of the transcendental method in the partially magnetized regime where, as opposed to $\beta^2_{\rm eff} \gg 1$ ($\beta^2_{\rm eff} \ll 1$), the effective electric field is not trivially $E_{\rm eff} = E_\parallel$ ($E_{\rm eff} = E$). In what follows, $\omega_{\rm ce}/N \simeq 10^{-13}$ rad m^3 s^{-1} (for all gases), which is close to the $(\omega_{\rm ce}/N)_2$ value in figure 3 and corresponds to partially magnetized electrons. The quantities used for comparison are the mean energy of electrons $\varepsilon_{\rm m}$, the electron impact ionization frequency $\nu_{\rm i}$, the mobility parallel to the magnetic field $\mu_\parallel$, and the mobility perpendicular to the magnetic field $\mu_\perp$. This choice of comparisons has been made to investigate the performance of the proposed transcendental method as it pertains to both the f_0 and $\vec{f}_1$ terms in the two-term expansion of the EVDF.

Figures 4–6 respectively depict comparisons in gas mixtures (1)–(3). All panels include $\beta_{\rm eff} = (\omega_{\rm ce}/N)/k_{\rm m}(E_{\rm eff}/N)$ after finding the solution to equation (1) to illustrate the degree of magnetization of the electrons. It is inferred from these figures that the transcendental method for $w = w_3$ and the approximation to this method agree to a satisfactory degree. In addition, both methods agree with the exact calculations of BOLSIG+ for the majority of the E/N range. Thus, the interested reader may initially implement the simpler approximate transcendental method presented in section 2 to evaluate and explore the method's performance for an arbitrary gas mixture.

The observed deviation of $\nu_{\rm i}$ results of BOLSIG+ from that of both transcendental methods at $\angle\vec{E},\vec{B} = 90°$ (i.e. $E_\parallel = 0$) is generally considerable. On the other hand, the agreement between $\varepsilon_{\rm m}$ calculated for the same scenario by all methods is satisfactory. This observation emphasizes the difference in the high energy tail of the exact EEDF calculated by BOLSIG+ for $\vec{B} \neq 0$ and the EEDFs (corresponding to $\vec{B} = 0$) used in the transcendental methods. Specifically, both $\varepsilon_{\rm m}$ and $\nu_{\rm i}$ depend on the isotropic term of the EVDF. However, the latter involves, exclusively, the high-energy electrons represented in the tail of the EEDF (vs ε) since electron impact ionization is a collision with an energy threshold. While the abundance of these ionizing electrons

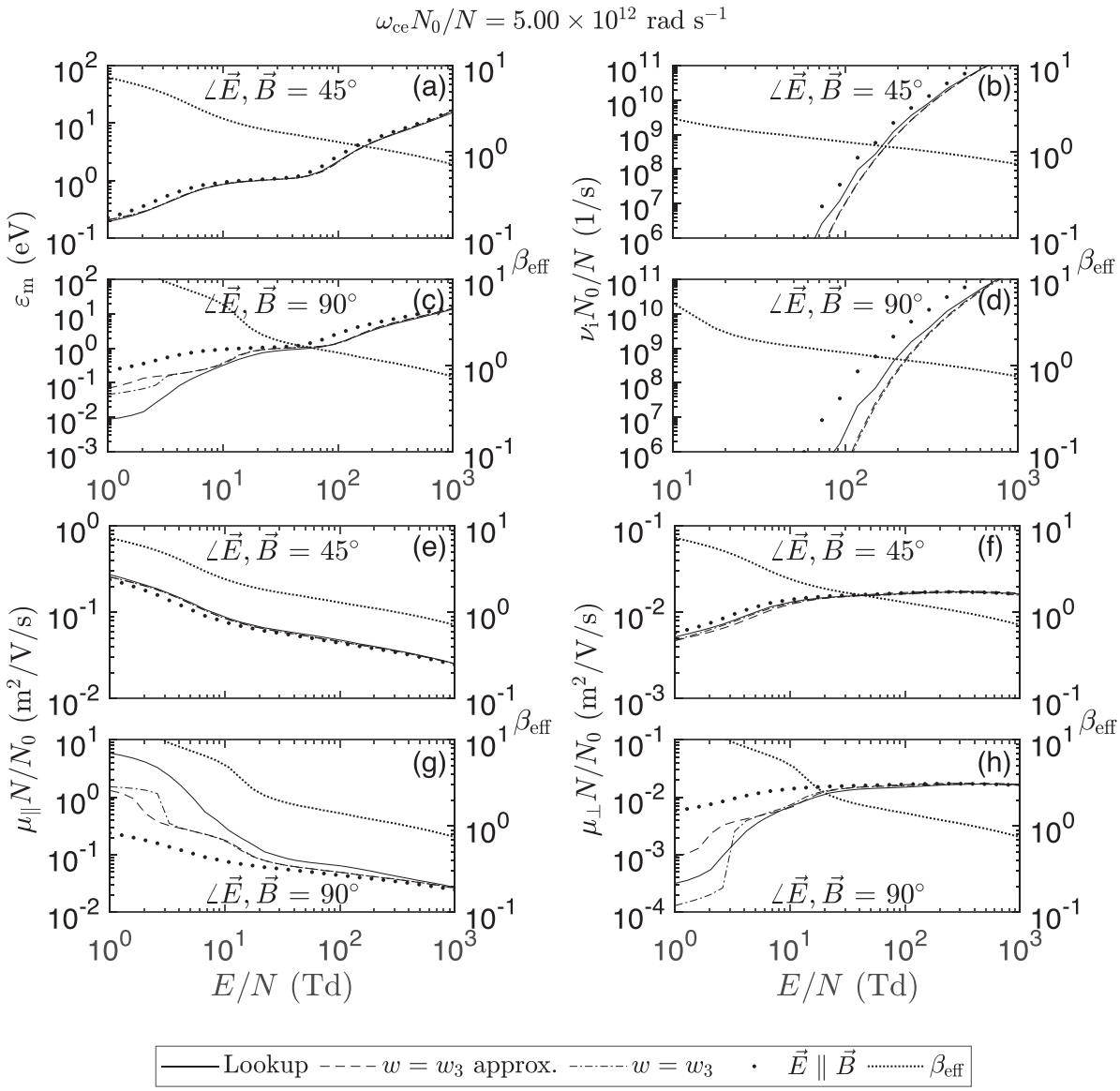

Figure 4. (a) Electron mean energy and (b) electron impact ionization frequency for $\angle\vec{E},\vec{B} = 45°$. (c) Electron mean energy and (d) electron impact ionization frequency for $\angle\vec{E},\vec{B} = 90°$. Mobility of electrons (e) parallel and (f) perpendicular to $\vec{B}$ for $\angle\vec{E},\vec{B} = 45°$. Mobility of electrons (g) parallel and (h) perpendicular to $\vec{B}$ for $\angle\vec{E},\vec{B} = 90°$. Results are for air.

controls the ionization rate constant, their exponentially lower population compared to low-energy electrons results in a negligible impact on the ε_m values presented. We note that the same analysis is true for rate constants of other electron impact processes with an energy threshold. The disagreement is more pronounced for electron impact collisions with a higher energy threshold.

Values corresponding to $\vec{E} \parallel \vec{B}$ are also included in all panels. Specifically, the extremely low ionization levels when $\angle\vec{E},\vec{B} = 90°$ are demonstrated. While $\angle\vec{E},\vec{B} = 90°$ corresponds to the lowest agreement between ν_i results of BOLSIG+ and the transcendental methods, the exact results of BOLSIG+ are still orders of magnitude less than scenarios in which $\angle\vec{E},\vec{B} \to 0$. We note that this holds even for $\angle\vec{E},\vec{B}$ as high as 45° (see panels (b) and (d) in figures 4–6). As such, one may conclude that in a realistic scenario where $\angle\vec{E},\vec{B}$ may vary in the entire range of $\angle\vec{E},\vec{B} = 0 - 90°$, even exact ν_i values corresponding to $\angle\vec{E},\vec{B} = 90°$ are so insignificant that the disagreement between BOLSIG+ and the transcendental methods has no practical significance in the framework of plasma fluid models in which these coefficients are typically employed (e.g. Starikovskiy *et al* 2021, Janalizadeh and Pasko 2023). In other words, unless in the entire simulation domain $\angle\vec{E},\vec{B} \to 90°$ and the process involves electric fields close to E_k (as the threshold for significant ionization), the transcendental method provides accurate results for the ionization frequency. A similar argument may be made for the parallel mobility panel in

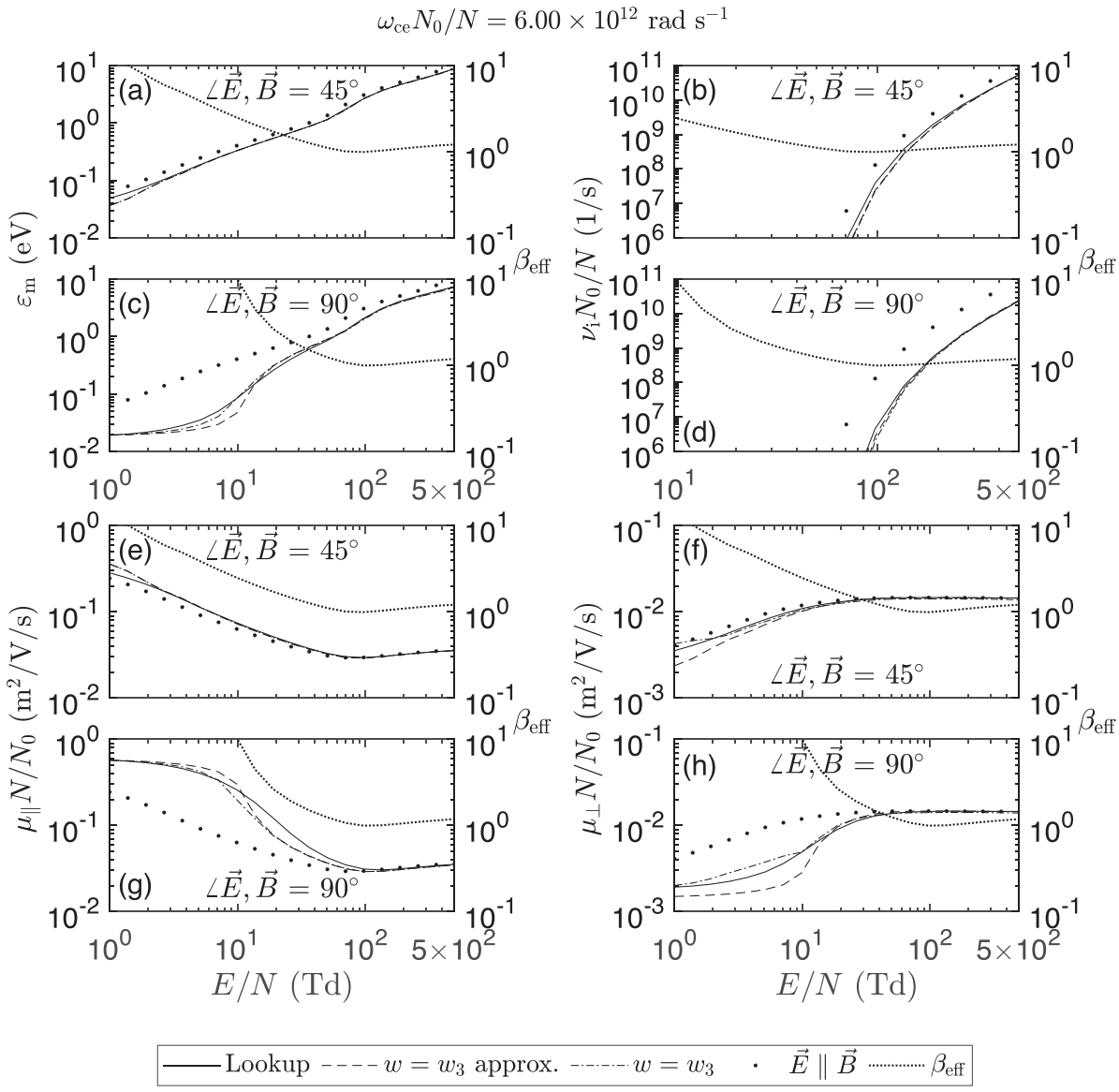

Figure 5. (a) Electron mean energy and (b) electron impact ionization frequency for $\angle\vec{E},\vec{B} = 45°$. (c) Electron mean energy and (d) electron impact ionization frequency for $\angle\vec{E},\vec{B} = 90°$. Mobility of electrons (e) parallel and (f) perpendicular to $\vec{B}$ for $\angle\vec{E},\vec{B} = 45°$. Mobility of electrons (g) parallel and (h) perpendicular to $\vec{B}$ for $\angle\vec{E},\vec{B} = 90°$. Results are for a mixture of 88% H_2 and 12% He.

figure 4, i.e. figure 4(g), where one observes a clear disagreement between the BOLSIG+ exact results and both transcendental methods in the low E/N region. Specifically, in this case, $E_\parallel = 0$ such that the drift of electrons parallel to $\vec{B}$ is absent. As for $\mu_\perp$ depicted in figure 4(h), one can clearly infer the better performance of the exact transcendental method (i.e. $w = w_3$) compared to the approximate transcendental method described in section 2.

The results succinctly depicted in figures 4–6 may be presented in a different format. Specifically, they can be presented as two-dimensional color plots that cover the entire range of $\angle\vec{E},\vec{B} = 0 - 90°$ and $\omega_{ce}/N \in [(\omega_{ce}/N)_1, (\omega_{ce}/N)_3] = [10^{-14}, 10^{-12}]$ rad m^3 s^{-1} for a select few applied reduced fields E/N. In that case, one may initiate the transcendental method and BOLSIG+ calculations since $(E/N, \omega_{ce}/N, \angle\vec{E},\vec{B})$ is now defined. Subsequently, a quantitative error that provides the percentage difference between BOLSIG+ and the transcendental method by normalizing it to BOLSIG+ exact values may be introduced. Due to the general satisfactory performance of the approximate transcendental method and for the sake of brevity, such figures are included in the supplementary file that accompanies this paper.

At the end of this section, we emphasize that the presented results target the regime of partially magnetized plasma. One expects a better agreement between the transcendental method and BOLSIG+ exact calculations in both cases of essentially non-magnetized ($\beta_{eff}^2 \ll 1$) and fully magnetized ($\beta_{eff}^2 \gg 1$) plasma since in those cases $E_{eff} = E$ and $E_{eff} = E_\parallel$, respectively (see

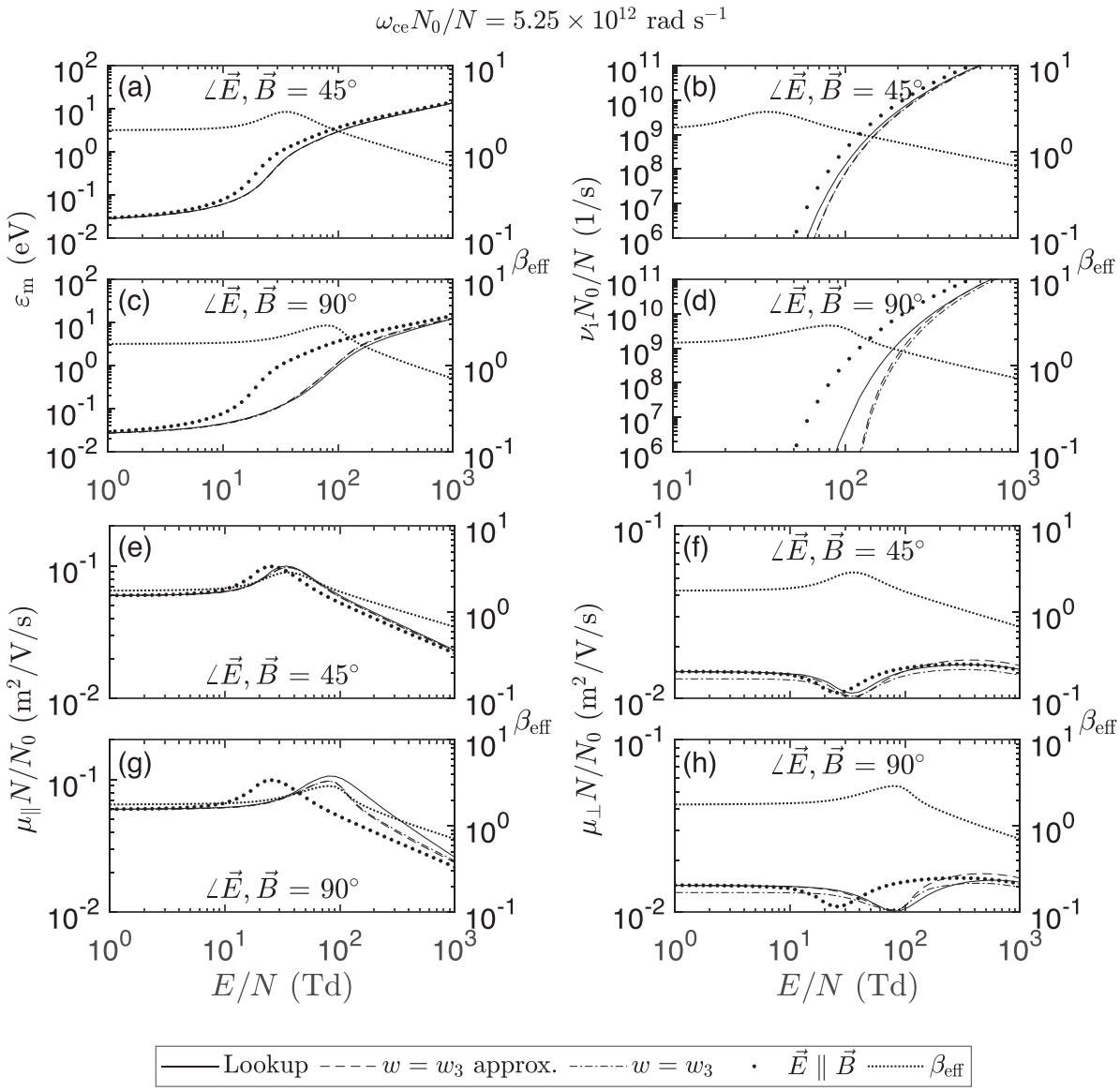

Figure 6. (a) Electron mean energy and (b) electron impact ionization frequency for $\angle\vec{E},\vec{B} = 45°$. (c) Electron mean energy and (d) electron impact ionization frequency for $\angle\vec{E},\vec{B} = 90°$. Mobility of electrons (e) parallel and (f) perpendicular to $\vec{B}$ for $\angle\vec{E},\vec{B} = 45°$. Mobility of electrons (g) parallel and (h) perpendicular to $\vec{B}$ for $\angle\vec{E},\vec{B} = 90°$. Results are for pure CO_2.

figure 2). An even more accurate transcendental method may be obtained by extending the presented model formulation to solutions of the Boltzmann equation that are more accurate than the two-term approximation.

5. Conclusions

We introduce a new transcendental approach to the calculation of electron transport and rate coefficients in a magnetized plasma using the theory and results of non-magnetized plasma. The obtained effective electric field results in plasma transport parameters that are in satisfactory agreement with BOLSIG+'s exact calculations in air, a mixture of 88% molecular hydrogen with 12% helium, and pure carbon dioxide. Furthermore, the effective electric field is in the same format as the electric field a single electron experiences in the presence of a magnetic field. This provides an intuitive picture, which accompanies the rigorous mathematical derivations presented here. Subsequently, a special case of the formulation is further explored to reduce calculations and use the electron rate and transport coefficients outputted by BOLSIG+. While as a result of the kinetic theory of weakly ionized and magnetized plasma the electron transport and rate coefficients are defined through a distribution function that varies with $(E/N, \omega_{ce}/N, \angle\vec{E},\vec{B})$, the new method proceeds in two steps: (1) the calculation of E_{eff} for a given $(E/N, \omega_{ce}/N, \angle\vec{E},\vec{B})$ through a simple transcendental equation, and (2) the calculation of electron transport and rate coefficients in the absence of a magnetic field using E_{eff}/N (since when $\vec{B} = 0$, the transport parameters become functions of E_{eff}/N, exclusively).

Data availability statement

All data that support the findings of this study are included within the article (and any supplementary files).

Acknowledgments

This research was supported by NSF under Grants AGS-1744099 and AGS-2010088 to Penn State University.

Appendix A. Theory of general transcendental method and minimum error value

In this section we start with the definition of the error function introduced in equation (6). Using the residual $R(v)$ given by equation (5), we have

$$\frac{\partial \mathcal{E}}{\partial E_{\rm eff}} = \int_{v=0}^{\infty} \frac{1}{9}\left(\frac{q_{\rm e}}{m_{\rm e}}\right)^4 \frac{1}{v^4}(2) \times \left\{\frac{\partial}{\partial v}\left[\left(\frac{E_\perp^2}{1+\beta_{\rm H}^2(v)} + E_\parallel^2 - E_{\rm eff}^2\right)\frac{v^2}{\nu_{\rm m}(v)}\frac{\partial f_0}{\partial v}\right]\right\} \cdot \frac{\partial}{\partial E_{\rm eff}}\left\{\frac{\partial}{\partial v}\left[\left(\frac{E_\perp^2}{1+\beta_{\rm H}^2(v)} + E_\parallel^2 - E_{\rm eff}^2\right) \times \frac{v^2}{\nu_{\rm m}(v)}\frac{\partial f_0}{\partial v}\right]\right\} w(v)\,{\rm d}v. \tag{A.1}$$

Since $\frac{\partial}{\partial E_{\rm eff}}\frac{\partial}{\partial v}(\cdot) = \frac{\partial}{\partial v}\frac{\partial}{\partial E_{\rm eff}}(\cdot)$, we have

$$\frac{\partial}{\partial E_{\rm eff}}\left\{\frac{\partial}{\partial v}\left[\left(\frac{E_\perp^2}{1+\beta_{\rm H}^2(v)} + E_\parallel^2 - E_{\rm eff}^2\right)\frac{v^2}{\nu_{\rm m}(v)}\frac{\partial f_0}{\partial v}\right]\right\} = -2E_{\rm eff}\frac{\partial}{\partial v}\left[\frac{v^2}{\nu_{\rm m}(v)}\frac{\partial f_0}{\partial v}\right]. \tag{A.2}$$

We note that based on the definition of EVDF, f_0 here is only a function of v and therefore, $\frac{\partial f_0}{\partial E_{\rm eff}} = 0$. Consequently,

$$0 = \frac{\partial \mathcal{E}}{\partial E_{\rm eff}} = -\frac{4}{9}\left(\frac{q_{\rm e}}{m_{\rm e}}\right)^4 E_{\rm eff}\int_{v=0}^{\infty}\frac{1}{v^4} \times \left\{\frac{\partial}{\partial v}\left[\left(\frac{E_\perp^2}{1+\beta_{\rm H}^2(v)} + E_\parallel^2 - E_{\rm eff}^2\right)\frac{v^2}{\nu_{\rm m}(v)}\frac{\partial f_0}{\partial v}\right]\right\} \cdot \frac{\partial}{\partial v}\left[\frac{v^2}{\nu_{\rm m}(v)}\frac{\partial f_0}{\partial v}\right] w(v)\,{\rm d}v. \tag{A.3}$$

Since the trivial solution $E_{\rm eff} = 0$ is unacceptable, we should have

$$\int_{v=0}^{\infty}{\rm d}v\frac{w(v)}{v^4}\left\{\frac{\partial}{\partial v}\left[\left(\frac{E_\perp^2}{1+\beta_{\rm H}^2(v)}\right)\left(\frac{v^2}{\nu_{\rm m}(v)}\frac{\partial f_0}{\partial v}\right)\right] + \left(E_\parallel^2 - E_{\rm eff}^2\right)\frac{\partial}{\partial v}\left(\frac{v^2}{\nu_{\rm m}(v)}\frac{\partial f_0}{\partial v}\right)\right\} \cdot \left\{\frac{\partial}{\partial v}\left[\frac{v^2}{\nu_{\rm m}(v)}\frac{\partial f_0}{\partial v}\right]\right\} = 0 \tag{A.4}$$

where we used the fact that

$$\frac{\partial}{\partial v}\left[\left(\frac{E_\perp^2}{1+\beta_{\rm H}^2(v)} + E_\parallel^2 - E_{\rm eff}^2\right)\frac{v^2}{\nu_{\rm m}(v)}\frac{\partial f_0}{\partial v}\right] = \frac{\partial}{\partial v}\left[\left(\frac{E_\perp^2}{1+\beta_{\rm H}^2(v)}\right)\left(\frac{v^2}{\nu_{\rm m}(v)}\frac{\partial f_0}{\partial v}\right)\right] + \left(E_\parallel^2 - E_{\rm eff}^2\right)\frac{\partial}{\partial v}\left(\frac{v^2}{\nu_{\rm m}(v)}\frac{\partial f_0}{\partial v}\right). \tag{A.5}$$

Distributing the integral among the two terms above and defining I_1 and I_2 as

$$I_1 = \int_{v=0}^{\infty}\left[\frac{1}{v^2}\frac{\partial}{\partial v}\left(\frac{v^2}{\nu_{\rm m}(v)}\frac{\partial f_0}{\partial v}\right)\right]^2 w(v){\rm d}v \tag{A.6}$$

and

$$I_2 = \int_{v=0}^{\infty}\left[\frac{1}{v^2}\frac{\partial}{\partial v}\left(\frac{1}{1+\beta_{\rm H}^2(v)}\frac{v^2}{\nu_{\rm m}(v)}\frac{\partial f_0}{\partial v}\right)\right] \cdot \left[\frac{1}{v^2}\frac{\partial}{\partial v}\left(\frac{v^2}{\nu_{\rm m}(v)}\frac{\partial f_0}{\partial v}\right)\right] w(v){\rm d}v \tag{A.7}$$

respectively, we arrive at

$$E_\perp^2 I_2 = \left(E_{\rm eff}^2 - E_\parallel^2\right) I_1. \tag{A.8}$$

Thus,

$$E_{\rm eff}^2 = E_\parallel^2 + E_\perp^2\frac{I_2}{I_1} = E_\parallel^2 + \frac{E_\perp^2}{\frac{I_1}{I_2}} = E_\parallel^2 + \frac{E_\perp^2}{1+\beta_{\rm eff}^2}. \tag{A.9}$$

Using the equation above, the residual corresponding to the minimum error may be expressed as

$$R_{\rm min}(v) = \frac{1}{3}\left(\frac{q_{\rm e}E}{m_{\rm e}}\right)^2\frac{\sin^2(\angle\vec{E},\vec{B})}{v^2}\frac{\partial}{\partial v} \times \left[\left(\frac{1}{1+\beta_{\rm H}^2(v)} - \frac{1}{1+\beta_{\rm eff}^2}\right)\frac{v^2}{\nu_{\rm m}(v)}\frac{\partial f_0}{\partial v}\right] \tag{A.10}$$

where we have used $E_\perp = E\sin(\angle\vec{E},\vec{B})$. Subsequently, we have

$$\mathcal{E}_{\rm min} = \frac{1}{9}\left(\frac{q_{\rm e}E}{m_{\rm e}}\right)^4\sin^4(\angle\vec{E},\vec{B})\int_{v=0}^{\infty}{\rm d}v\frac{w(v)}{v^4} \times \left\{\frac{\partial}{\partial v}\left[\left(\frac{1}{1+\beta_{\rm H}^2(v)} - \frac{1}{1+\beta_{\rm eff}^2}\right)\frac{v^2}{\nu_{\rm m}(v)}\frac{\partial f_0}{\partial v}\right]\right\}^2 \tag{A.11}$$

where

$$\frac{\partial}{\partial v}\left[\left(\frac{1}{1+\beta_{\rm H}^2(v)} - \frac{1}{1+\beta_{\rm eff}^2}\right)\frac{v^2}{\nu_{\rm m}(v)}\frac{\partial f_0}{\partial v}\right] = \frac{\partial}{\partial v}\left[\frac{1}{1+\beta_{\rm H}^2(v)}\frac{v^2}{\nu_{\rm m}(v)}\frac{\partial f_0}{\partial v} - \frac{1}{1+\beta_{\rm eff}^2}\frac{v^2}{\nu_{\rm m}(v)}\frac{\partial f_0}{\partial v}\right] = \frac{\partial}{\partial v}\left(\frac{1}{1+\beta_{\rm H}^2(v)}\frac{v^2}{\nu_{\rm m}(v)}\frac{\partial f_0}{\partial v}\right) - \frac{1}{1+\beta_{\rm eff}^2}\frac{\partial}{\partial v}\left(\frac{v^2}{\nu_{\rm m}(v)}\frac{\partial f_0}{\partial v}\right). \tag{A.12}$$

Since

$$\left[\frac{\partial}{\partial v}\left(\frac{1}{1+\beta_{\rm H}^2(v)}\frac{v^2}{\nu_{\rm m}(v)}\frac{\partial f_0}{\partial v}\right)-\frac{1}{1+\beta_{\rm eff}^2}\frac{\partial}{\partial v}\left(\frac{v^2}{\nu_{\rm m}(v)}\frac{\partial f_0}{\partial v}\right)\right]^2 = \left[\frac{\partial}{\partial v}\left(\frac{1}{1+\beta_{\rm H}^2(v)}\frac{v^2}{\nu_{\rm m}(v)}\frac{\partial f_0}{\partial v}\right)\right]^2-\frac{2}{1+\beta_{\rm eff}^2}\frac{\partial}{\partial v} \times\left(\frac{1}{1+\beta_{\rm H}^2(v)}\frac{v^2}{\nu_{\rm m}(v)}\frac{\partial f_0}{\partial v}\right)\frac{\partial}{\partial v}\left(\frac{v^2}{\nu_{\rm m}(v)}\frac{\partial f_0}{\partial v}\right) +\left[\frac{1}{1+\beta_{\rm eff}^2}\frac{\partial}{\partial v}\left(\frac{v^2}{\nu_{\rm m}(v)}\frac{\partial f_0}{\partial v}\right)\right]^2 \tag{A.13}$$

defining I_3 as

$$I_3=\int_{v=0}^{\infty}\left[\frac{1}{v^2}\frac{\partial}{\partial v}\left(\frac{1}{1+\beta_{\rm H}^2(v)}\frac{v^2}{\nu_{\rm m}(v)}\frac{\partial f_0}{\partial v}\right)\right]^2 w(v)\mathrm{d}v \tag{A.14}$$

results in

$$\mathcal{E}_{\rm min}=\frac{1}{9}\left(\frac{q_{\rm e}E}{m_{\rm e}}\right)^4\sin^4(\angle\vec{E},\vec{B})\left[I_3-\frac{2}{1+\beta_{\rm eff}^2}I_2+\frac{1}{(1+\beta_{\rm eff}^2)^2}I_1\right]. \tag{A.15}$$

Equivalently,

$$\mathcal{E}_{\rm min}=\frac{1}{9}\left(\frac{q_{\rm e}E}{m_{\rm e}}\right)^4\sin^4(\angle\vec{E},\vec{B})I_2\left[\frac{I_3}{I_2}-\frac{I_2}{I_1}\right] \tag{A.16}$$

where we have used $1+\beta_{\rm eff}^2=I_1/I_2$. While $\mathcal{E}_{\rm min}$ depends on $\angle\vec{E},\vec{B}$ implicitly through determination of $\beta_{\rm eff}$ for any set of input parameters, one can also see the explicit dependence on $\angle\vec{E},\vec{B}$ through the $\sin^4(\angle\vec{E},\vec{B})$ factor. Assuming the variation of the latter as a function of $\angle\vec{E},\vec{B}$ is the dominant factor (see figures 4–6 for illustrations of negligible $\beta_{\rm eff}$ variation as a function of $\angle\vec{E},\vec{B}$), one concludes that the error of the transcendental method increases monotonically with $\angle\vec{E},\vec{B}$ such that the maximum discrepancy in comparison with the exact calculations occurs at $\angle\vec{E},\vec{B}=90^\circ$.

Appendix B. Simplified transcendental method when $w(v)=w_3(v)$

Using $w_3(v)$ as defined in equation (8) and applying integration by parts to I_1, we have

$$I_1^{w_3}=\int_{v=0}^{\infty}v^2\left[\frac{\partial}{\partial v}\left(\frac{v^2}{\nu_{\rm m}(v)}\frac{\partial f_0}{\partial v}\right)\right]\mathrm{d}v =\frac{v^4}{\nu_{\rm m}(v)}\frac{\partial f_0}{\partial v}\bigg|_{v=0}^{\infty}-2\int_{v=0}^{\infty}\frac{v^3}{\nu_{\rm m}(v)}\frac{\partial f_0}{\partial v}\mathrm{d}v=C_1^{w_3}\bigg|_{v=0}^{\infty}-2I_{1,1}^{w_3}. \tag{B.1}$$

Before demonstrating that $I_{1,1}^{w_3}$ is proportional to $\mu_\parallel$, i.e. electron mobility parallel to the magnetic field (when $B\neq0$), we show that $C_1^{w_3}(v=\infty)=0$. Let's assume there is at least a single constant $k>0$ for which one can find a constant v_0 so that the inequality $0\leqslant v^\ell\leqslant kf_0(v)4\pi v^2$ holds for $v>v_0$. In other words, $v^\ell\in O[f_0(v)4\pi v^2]$. Then,

$$n_{\rm e}=\int_{v=0}^{\infty}f_0(v)4\pi v^2\mathrm{d}v=\int_{v=0}^{v_0}f_0(v)4\pi v^2\mathrm{d}v+\int_{v=v_0}^{\infty}f_0(v)4\pi v^2\mathrm{d}v \tag{B.2}$$

and based on the inequality introduced above,

$$\int_{v=0}^{v_0}f_0(v)4\pi v^2\mathrm{d}v+\frac{1}{k}\int_{v=v_0}^{\infty}v^\ell\mathrm{d}v\leqslant n_{\rm e}. \tag{B.3}$$

Note that $n_{\rm e}-\int_{v=0}^{v_0}f_0(v)4\pi v^2\mathrm{d}v$ is a bounded positive quantity and therefore, the integral above including v^ℓ should be convergent. Introducing the change of variable $t=v/v_0$ we have $\int_{t=1}^{\infty}t^\ell\mathrm{d}t<\infty$, which occurs only if $\ell<-1$. Consequently, $f_0(v)\geqslant\frac{1}{4\pi k}v^{\ell-2}$, i.e. $f_0(v)$ falls off faster than v^{-3} as $v\to\infty$. This implies that as $v\to\infty$, $\frac{\partial f_0}{\partial v}$ falls off faster than v^{-4} such that $C_1^{w_3}(v\to\infty)$ falls off faster than v^{-1} since $\nu_{\rm m}(\varepsilon)=N\sigma_{\rm m}(\varepsilon)v=N\sigma_{\rm m}(\varepsilon)\gamma\varepsilon^{\frac{1}{2}}$. Thus, $C_1^{w_3}(v=\infty)=0$.

To be consistent with BOLSIG+'s definition of mobility (Hagelaar 2016, p 16), we now switch from v to ε to obtain

$$I_{1,1}^{w_3}=\int_{\varepsilon=0}^{\infty}\frac{\left(\gamma\varepsilon^{\frac{1}{2}}\right)^3}{\nu_{\rm m}(\varepsilon)}2\gamma^{-1}\varepsilon^{\frac{1}{2}}\frac{\partial}{\partial\varepsilon}\left[\frac{n_{\rm e}}{2\pi\gamma^3}F_0(\varepsilon)\right]\left(\frac{\gamma}{2}\varepsilon^{-\frac{1}{2}}\mathrm{d}\varepsilon\right) =\frac{1}{2\pi\gamma}\frac{n_{\rm e}}{N}\int_{\varepsilon=0}^{\infty}\frac{\varepsilon}{\sigma_{\rm m}(\varepsilon)}\frac{\partial F_0}{\partial\varepsilon}\mathrm{d}\varepsilon. \tag{B.4}$$

In Hagelaar (2016, p 16) we have mobility parallel to the magnetic field defined as

$$\mu_\parallel N=-\frac{\gamma}{3}\int_{\varepsilon=0}^{\infty}\frac{\varepsilon}{\sigma_{\rm m}(\varepsilon)}\frac{\partial F_0}{\partial\varepsilon}\mathrm{d}\varepsilon \tag{B.5}$$

such that

$$I_{1,1}^{w_3}=-\frac{3}{2\pi}\gamma^{-2}n_{\rm e}\mu_\parallel\to I_1^{w_3}=\frac{3}{\pi}\gamma^{-2}n_{\rm e}\mu_\parallel. \tag{B.6}$$

Similarly for $I_2^{w_3}$ we have

$$I_2^{w_3}=\int_{v=0}^{\infty}v^2\frac{\partial}{\partial v}\left[\frac{1}{1+\beta_{\rm H}^2(v)}\frac{v^2}{\nu_{\rm m}(v)}\frac{\partial f_0}{\partial v}\right]\mathrm{d}v =\frac{1}{1+\beta_{\rm H}^2(v)}\frac{v^4}{\nu_{\rm m}(v)}\frac{\partial f_0}{\partial v}\bigg|_{v=0}^{\infty}-2 \times\int_{v=0}^{\infty}\frac{1}{1+\beta_{\rm H}^2(v)}\frac{v^3}{\nu_{\rm m}(v)}\frac{\partial f_0}{\partial v}\mathrm{d}v=C_2^{w_3}\bigg|_{v=0}^{\infty}-2I_{2,1}^{w_3}. \tag{B.7}$$

The same arguments detailed above result in $C_2^{w_3}(v=\infty)=0$ and

$$I_2^{w_3}=\frac{3}{\pi}\gamma^{-2}n_{\rm e}\mu_\perp^0 \tag{B.8}$$

where $\mu_\perp^0$ is in the same format of perpendicular mobility

$$\mu_\perp N=-\frac{\gamma}{3}\int_{\varepsilon=0}^{\infty}\frac{1}{1+\beta_{\rm H}^2(\varepsilon)}\frac{\varepsilon}{\sigma_{\rm m}(\varepsilon)}\frac{\partial F_0}{\partial\varepsilon}\mathrm{d}\varepsilon \tag{B.9}$$

defined in Hagelaar (2016, p 16). In conclusion, for $w = w_3$, the simpler transcendental expression

$$E_{\text{eff}}^2 = E_{\parallel}^2 + \frac{E_{\perp}^2}{\left(\frac{\mu_{\parallel}}{\mu_{\perp}^0}\right)} \tag{B.10}$$

is derived in which $\mu_{\parallel}N$ is a function of E_{eff}/N exclusively, whereas $\mu_{\perp}^0 N$ is dependent on both E_{eff}/N and ω_{ce}/N. Note that $\mu_{\parallel}N$ is provided by BOLSIG+ and $\mu_{\perp}^0 N$ is calculated with the EEDF corresponding to $\vec{B} = 0$.

Appendix C. Simplified transcendental method when $w(v) = w_3(v)$ and $\beta_{\text{H}}^2(v) \gg 1$

A special case of the current version of the transcendental method is obtained when $\beta_{\text{H}}(\varepsilon) > 1$ such that $\beta_{\text{H}}^2(\varepsilon) \gg 1$. We start with

$$\begin{aligned}\mu_{\perp}^0 N &= -\frac{\gamma}{3}\int_{\varepsilon=0}^{\infty} \frac{1}{1+\beta_{\text{H}}^2(\varepsilon)} \frac{\varepsilon}{\sigma_{\text{m}}(\varepsilon)} \frac{\partial F_0}{\partial \varepsilon}\,\mathrm{d}\varepsilon \\ &\simeq -\frac{\gamma}{3}\int_{\varepsilon=0}^{\infty} \frac{1}{\beta_{\text{H}}^2(\varepsilon)} \frac{\varepsilon}{\sigma_{\text{m}}(\varepsilon)} \frac{\partial F_0}{\partial \varepsilon}\,\mathrm{d}\varepsilon.\end{aligned} \tag{C.1}$$

Since $\beta_{\text{H}}(\varepsilon) = \frac{\omega_{\text{ce}}}{\nu_{\text{m}}(\varepsilon)} = \frac{\omega_{\text{ce}}/N}{\sigma_{\text{m}}(\varepsilon)v} = \frac{\omega_{\text{ce}}/N}{\sigma_{\text{m}}(\varepsilon)\left(\gamma\varepsilon^{\frac{1}{2}}\right)}$, we have $\beta_{\text{H}}^{-2}(\varepsilon) = \frac{\gamma^2\sigma_{\text{m}}^2(\varepsilon)\varepsilon}{(\omega_{\text{ce}}/N)^2}$ and

$$\begin{aligned}\mu_{\perp}^0 N &\simeq -\frac{\gamma^3}{3}\int_{\varepsilon=0}^{\infty} \frac{\gamma^2\sigma_{\text{m}}^2(\varepsilon)\varepsilon}{(\omega_{\text{ce}}/N)^2} \frac{\varepsilon}{\sigma_{\text{m}}(\varepsilon)} \frac{\partial F_0}{\partial \varepsilon}\,\mathrm{d}\varepsilon \\ &= -\frac{\gamma^3}{3}\left(\frac{\omega_{\text{ce}}}{N}\right)^{-2}\int_{\varepsilon=0}^{\infty} \varepsilon^2\sigma_{\text{m}}(\varepsilon) \frac{\partial F_0}{\partial \varepsilon}\,\mathrm{d}\varepsilon.\end{aligned} \tag{C.2}$$

Using $\sigma_{\text{m}}(\varepsilon)v = \sigma_{\text{m}}(\varepsilon)\gamma\varepsilon^{\frac{1}{2}}$, we have

$$\mu_{\perp}^0 N \simeq -\frac{\gamma^3}{3}\left(\frac{\omega_{\text{ce}}}{N}\right)^{-2}\int_{\varepsilon=0}^{\infty} \frac{1}{\gamma}\left(\gamma\varepsilon^{\frac{1}{2}}\sigma_{\text{m}}(\varepsilon)\right)\left(\varepsilon^{\frac{3}{2}}\frac{\partial F_0}{\partial \varepsilon}\right)\mathrm{d}\varepsilon. \tag{C.3}$$

Since $P_0(\varepsilon) = \varepsilon^{\frac{1}{2}}F_0(\varepsilon)$, where $\int_{\varepsilon=0}^{\infty} P_0(\varepsilon)\mathrm{d}\varepsilon = 1$ (see next section) and $\frac{\partial}{\partial\varepsilon}\left(\varepsilon^{\frac{3}{2}}F_0\right) = \frac{\partial\varepsilon^{\frac{3}{2}}}{\partial\varepsilon}F_0(\varepsilon) + \varepsilon^{\frac{3}{2}}\frac{\partial F_0}{\partial\varepsilon} \to \frac{\partial}{\partial\varepsilon}(\varepsilon P_0) = \frac{3}{2}\varepsilon^{\frac{1}{2}}F_0(\varepsilon) + \varepsilon^{\frac{3}{2}}\frac{\partial F_0}{\partial\varepsilon} = \frac{3}{2}P_0(\varepsilon) + \varepsilon^{\frac{3}{2}}\frac{\partial F_0}{\partial\varepsilon}$, we have

$$\mu_{\perp}^0 N \simeq -\frac{\gamma^2}{3}\left(\frac{\omega_{\text{ce}}}{N}\right)^{-2}\left[\gamma\int_{\varepsilon=0}^{\infty}\varepsilon^{\frac{1}{2}}\sigma_{\text{m}}(\varepsilon)\frac{\partial(\varepsilon P_0)}{\partial\varepsilon}\,\mathrm{d}\varepsilon - \frac{3}{2}\frac{\nu_{\text{m}}}{N}\right] \tag{C.4}$$

where for the second integral we used the definition of momentum transfer collision frequency $\nu_{\text{m}} \equiv \int_{\varepsilon=0}^{\infty}(N\sigma_{\text{m}}(\varepsilon)v)\,P_0(\varepsilon)\mathrm{d}\varepsilon$. Using integration by parts for the first integral in the brackets, we obtain

$$\begin{aligned}&\int_{\varepsilon=0}^{\infty}\sigma_{\text{m}}(\varepsilon)\varepsilon^{\frac{1}{2}}\frac{\partial(\varepsilon P_0)}{\partial\varepsilon}\,\mathrm{d}\varepsilon \\ &= \left(\sigma_{\text{m}}(\varepsilon)\varepsilon^{\frac{1}{2}}\right)\varepsilon P_0\Big|_{\varepsilon=0}^{\infty} - \int_{\varepsilon=0}^{\infty}\varepsilon P_0(\varepsilon)\frac{\partial}{\partial\varepsilon}\left(\sigma_{\text{m}}(\varepsilon)\varepsilon^{\frac{1}{2}}\right)\mathrm{d}\varepsilon\end{aligned} \tag{C.5}$$

where the limit term vanishes due to arguments similar to those made in the previous section and the integral term may be expressed as

$$\int_{\varepsilon=0}^{\infty}\varepsilon\frac{\partial}{\partial\varepsilon}\left(\sigma_{\text{m}}(\varepsilon)\varepsilon^{\frac{1}{2}}\right)P_0(\varepsilon)\mathrm{d}\varepsilon \equiv \left\langle\varepsilon\frac{\partial}{\partial\varepsilon}\left(\sigma_{\text{m}}(\varepsilon)\varepsilon^{\frac{1}{2}}\right)\right\rangle. \tag{C.6}$$

The average $\langle\varepsilon\frac{\partial}{\partial\varepsilon}\left(\sigma_{\text{m}}(\varepsilon)\varepsilon^{\frac{1}{2}}\right)\rangle$ is a measure of the variation of momentum transfer collision frequency as a function of electron energy. That is, $\sigma_{\text{m}}(\varepsilon) \propto \varepsilon^{-\frac{1}{2}}$ for which the average is identically zero corresponds to a constant momentum transfer collision frequency since $\nu_{\text{m}}(\varepsilon) = N\sigma_{\text{m}}(\varepsilon)v \propto \varepsilon^{-\frac{1}{2}}\left(\gamma\varepsilon^{\frac{1}{2}}\right) = \text{const}$. Assuming the average $\langle\varepsilon\frac{\partial}{\partial\varepsilon}\left(\sigma_{\text{m}}(\varepsilon)\varepsilon^{\frac{1}{2}}\right)\rangle$ is negligible,

$$\mu_{\perp}^0 N \simeq -\frac{\gamma^2}{3}\left(\frac{\omega_{\text{ce}}}{N}\right)^{-2}\left(-\frac{3}{2}\right)\frac{\nu_{\text{m}}}{N} = \frac{\gamma^2}{2}\left(\frac{\omega_{\text{ce}}}{N}\right)^{-2}\left(\frac{\nu_{\text{m}}}{N}\right) \tag{C.7}$$

such that

$$\begin{aligned}\frac{\mu_{\parallel}}{\mu_{\perp}^0} = \frac{\mu_{\parallel}N}{\mu_{\perp}^0 N} &= \frac{\left(\frac{\gamma^2}{2}\right)\left(\frac{\nu_{\text{m}}}{N}\right)^{-1}}{\frac{\gamma^2}{2}\left(\frac{\omega_{\text{ce}}}{N}\right)^{-2}\left(\frac{\nu_{\text{m}}}{N}\right)} = \frac{\left(\frac{\omega_{\text{ce}}}{N}\right)^2}{\left(\frac{\nu_{\text{m}}}{N}\right)^2} \\ &= \left(\frac{\omega_{\text{ce}}}{\nu_{\text{m}}}\right)^2 \simeq 1 + \left(\frac{\omega_{\text{ce}}}{\nu_{\text{m}}}\right)^2\end{aligned} \tag{C.8}$$

where in the final equality we used the fact that $\beta_{\text{H}}^2(\varepsilon) \gg 1$ implies $\nu_{\text{m}}(\varepsilon) < \omega_{\text{ce}}$ such that $\nu_{\text{m}} = \int_{\varepsilon=0}^{\infty}\nu_{\text{m}}(\varepsilon)P_0(\varepsilon)\mathrm{d}\varepsilon < \omega_{\text{ce}}$, and therefore, $\beta_{\text{eff}}^2 \gg 1$. Also, by definition, $\nu_{\text{m}}/N = \frac{q_{\text{e}}}{m_{\text{e}}(\mu_{\parallel}N)} = (q_{\text{e}}/m_{\text{e}})/(\mu_{\parallel}N) = (\gamma^2/2)/(\mu_{\parallel}N)$, where ν_{m}/N is the rate constant for momentum transfer when $\vec{B} = 0$, which varies only as a function of E_{eff}/N. In conclusion,

$$E_{\text{eff}}^2 = E_{\parallel}^2 + \frac{E_{\perp}^2}{\left(\frac{\mu_{\parallel}}{\mu_{\perp}^0}\right)} = E_{\parallel}^2 + \frac{E_{\perp}^2}{1+\left(\frac{\omega_{\text{ce}}}{\nu_{\text{m}}}\right)^2} = E_{\parallel}^2 + \frac{E_{\perp}^2}{1+\beta_{\text{eff}}^2}. \tag{C.9}$$

Appendix D. I_1 and I_2 integrals in terms of BOLSIG+ (Hagelaar and Pitchford 2005) variables

In Hagelaar and Pitchford (2005) we have $\gamma \equiv \left(\frac{2q_{\text{e}}}{m_{\text{e}}}\right)^{\frac{1}{2}}$, such that $v^2 = \gamma^2\varepsilon$ where, as defined earlier, ε denotes the electron energy in eV. Consequently, $v = \gamma\varepsilon^{\frac{1}{2}}$ and $\mathrm{d}v = \frac{\gamma}{2}\varepsilon^{-\frac{1}{2}}\mathrm{d}\varepsilon$. Thus, $\frac{\partial}{\partial v}(\cdot) = \frac{\partial}{\partial\varepsilon}(\cdot)\frac{\partial\varepsilon}{\partial v} = 2\gamma^{-1}\varepsilon^{\frac{1}{2}}\frac{\partial}{\partial\varepsilon}(\cdot)$ since $\varepsilon = \gamma^{-2}v^2$, $\frac{\partial\varepsilon}{\partial v} = 2\gamma^{-2}v = 2\gamma^{-2}(\gamma\varepsilon^{\frac{1}{2}}) = 2\gamma^{-1}\varepsilon^{\frac{1}{2}}$. The EEDF in BOLSIG+, i.e. $F_0(\varepsilon)$ is related to $f_0(v)$ via $f_0(v) = \frac{n_{\text{e}}}{2\pi\gamma^3}F_0(\varepsilon)$, where n_{e} denotes electron density. The EPDF in the present work is defined as $P_0(\varepsilon) = \varepsilon^{\frac{1}{2}}F_0(\varepsilon)$ such that $\int_{\varepsilon}P_0(\varepsilon)\,\mathrm{d}\varepsilon = 1$. Defining $W(\varepsilon)$ such that $W(\varepsilon)\mathrm{d}\varepsilon \equiv w(v)\mathrm{d}v$, we have

$$\frac{W(\varepsilon)}{w(v)} = \frac{\mathrm{d}v}{\mathrm{d}\varepsilon} = \frac{\gamma}{2}\varepsilon^{-\frac{1}{2}} \tag{D.1}$$

and the results in terms of ε and BOLSIG+'s EEDF may be expressed as

$$I_1 = \int_{\varepsilon=0}^{\infty} \left[\frac{1}{\gamma^2 \varepsilon} 2\gamma^{-1} \varepsilon^{\frac{1}{2}} \frac{\partial}{\partial \varepsilon} \left\{ \frac{\gamma^2 \varepsilon}{\nu_{\mathrm{m}}(\varepsilon)} 2\gamma^{-1} \varepsilon^{\frac{1}{2}} \frac{\partial}{\partial \varepsilon} \left(\frac{n_{\mathrm{e}}}{2\pi\gamma^3} F_0(\varepsilon) \right) \right\} \right]^2 \times W(\varepsilon) \mathrm{d}\varepsilon = \left(\frac{2}{\pi} \gamma^{-5} n_{\mathrm{e}} \right)^2 \int_{\varepsilon=0}^{\infty} \left[\frac{\partial}{\partial \varepsilon} \left\{ \frac{\varepsilon^{\frac{3}{2}}}{\nu_{\mathrm{m}}(\varepsilon)} \frac{\partial F_0}{\partial \varepsilon} \right\} \right]^2 \varepsilon^{-1} W(\varepsilon) \mathrm{d}\varepsilon \tag{D.2}$$

$$\begin{aligned} I_2 = \int_{\varepsilon=0}^{\infty} & \left\{ \frac{1}{\gamma^2 \varepsilon} 2\gamma^{-1} \varepsilon^{\frac{1}{2}} \frac{\partial}{\partial \varepsilon} \left[\frac{1}{1+\beta_{\mathrm{H}}^2(\varepsilon)} \frac{\gamma^2 \varepsilon}{\nu_{\mathrm{m}}(\varepsilon)} 2\gamma^{-1} \varepsilon^{\frac{1}{2}} \right. \right. \\ & \left. \left. \times \frac{\partial}{\partial \varepsilon} \left(\frac{n_{\mathrm{e}}}{2\pi\gamma^3} F_0(\varepsilon) \right) \right] \right\} \cdot \left\{ \frac{1}{\gamma^2 \varepsilon} 2\gamma^{-1} \varepsilon^{\frac{1}{2}} \frac{\partial}{\partial \varepsilon} \left[\frac{\gamma^2 \varepsilon}{\nu_{\mathrm{m}}(\varepsilon)} 2\gamma^{-1} \varepsilon^{\frac{1}{2}} \right. \right. \\ & \left. \left. \times \frac{\partial}{\partial \varepsilon} \left(\frac{n_{\mathrm{e}}}{2\pi\gamma^3} F_0(\varepsilon) \right) \right] \right\} W(\varepsilon) \mathrm{d}\varepsilon = \left(\frac{2}{\pi} \gamma^{-5} n_{\mathrm{e}} \right)^2 \\ & \times \int_{\varepsilon=0}^{\infty} \left\{ \frac{\partial}{\partial \varepsilon} \left[\frac{1}{1+\beta_{\mathrm{H}}^2(\varepsilon)} \frac{\varepsilon^{\frac{3}{2}}}{\nu_{\mathrm{m}}(\varepsilon)} \frac{\partial F_0}{\partial \varepsilon} \right] \right\} \\ & \times \left\{ \frac{\partial}{\partial \varepsilon} \left[\frac{\varepsilon^{\frac{3}{2}}}{\nu_{\mathrm{m}}(\varepsilon)} \frac{\partial F_0}{\partial \varepsilon} \right] \right\} \varepsilon^{-1} W(\varepsilon) \mathrm{d}\varepsilon. \end{aligned} \tag{D.3}$$

Note that since $\beta_{\mathrm{eff}} \propto \frac{I_1}{I_2}$, the absolute value of electron density or the constant γ is irrelevant in this analysis.

Appendix E. Existence and uniqueness of a convergent solution to equation (7)

In this section we answer the questions of existence and uniqueness of a convergent solution x to equation (7), repeated here as

$$x = \phi(x) \equiv \left[E_{\parallel}^2 + \frac{E_{\perp}^2}{1+\beta^2(x)} \right]^{\frac{1}{2}} \tag{E.1}$$

where we have used the change of symbol $E_{\mathrm{eff}} \to x$ and have dropped the subscript 'eff' from β_{eff} for the sake of brevity. By definition, x is a fixed point of the function $\phi(x)$, since from equation (E.1) we have $x = \phi(x)$. Since $\beta(x) \in C[0,E]$, where $C[a,b]$ is the space of all continuous functions in the interval $[a,b]$ and $a,b \in \mathbb{R}$, this implies $\phi(x) \in C[0,E]$ as well. It is clear from equation (E.1) that $\phi(x) \in [0,E]$, since $x \leqslant E$ always. The previous two statements imply that the function $\phi(\cdot)$ has a fixed point in the $[0,E]$ interval (Burden and Faires 2005, p 54, theorem 2.2a), and therefore, the question of the existence of a solution to equation (E.1) is answered. In addition, if $\phi'(x) = \mathrm{d}\phi/\mathrm{d}x$ in $(0,E)$ exists and so does a positive constant $k < 1$ such that

$$\left|\phi'(x)\right| \leqslant k \quad \text{for all } x \in (0,E) \tag{E.2}$$

then the fixed point in $[0,E]$ is unique (Burden and Faires 2005, p 54, theorem 2.2b).

The simple fixed-point iteration method can be used to solve equation (E.1) for x. The method starts with an initial approximation x_0 and then improves on this approximation using the recursive equation $x_{n+1} = \phi(x_n)$ until convergence is achieved. If condition (E.2) is satisfied, then it also ensures that for any initial value x_0, the sequence $\{x_n\}$ converges to the unique fixed point x (Burden and Faires 2005, p 58–59, theorem 2.3). Although checking condition (E.2) analytically might not be possible since $\beta(x)$ has a highly non-linear dependence on the electron energy distribution for any x, in the supplement to this paper we use numerical results to show that convergence is indeed achieved, provided the judicious choice of the initial value $x_0 = E$ is made (i.e. the applied electric field is used as the initial value for E_{eff} in the fixed-point iteration method to solve equations (1) and (7) or equation (E.1) here).

ORCID iDs

Reza Janalizadeh https://orcid.org/0000-0002-6014-2671
Victor P Pasko https://orcid.org/0000-0003-2675-6837

References

Barrington-Leigh C P, Inan U S and Stanley M 2001 Identification of sprites and elves with intensified video and broadband array photometry *J. Geophys. Res.: Space Phys.* **106** 1741–50
Bourdon A, Pasko V P, Liu N Y, Célestin S, Ségur P and Marode E 2007 Efficient models for photoionization produced by non-thermal gas discharges in air based on radiative transfer and the Helmholtz equations *Plasma Sources Sci. Technol.* **16** 656–78
Burden R L and Faires J D 2005 *Numerical Analysis* 8th edn (Belmont, CA: Thomson Brooks/Cole)
Dudley D G 1994 *Mathematical Foundations for Electromagnetic Theory* (Piscatawy, NJ: Wiley-IEEE Press)
Franz R C, Nemzek R J and Winckler J R 1990 Television image of a large upward electric discharge above a thunderstorm system *Science* **249** 48
Fukunishi H, Takahashi Y, Kubota M, Sakanoi K, Inan U S and Lyons W A 1996 Elves: lightning-induced transient luminous events in the lower ionosphere *Geophys. Res. Lett.* **23** 2157–60
Giles R S *et al* 2020 Possible transient luminous events observed in Jupiter's upper atmosphere *J. Geophys. Res.: Planets* **125** e2020JE006659
Golant V E, Zhilinsky A P and Sakharov I E 1980 *Fundamentals of Plasma Physics* (Hoboken, NJ: Wiley)
Hagelaar G J M 2016 *Brief Documentation of BOLSIG+ Version 03/2016* (Toulouse Cedex 9: Laboratoire Plasma et Conversion d'Energie (LAPLACE), Université Paul Sabatier)
Hagelaar G J M and Pitchford L C 2005 Solving the Boltzmann equation to obtain electron transport coefficients and rate coefficients for fluid models *Plasma Sources Sci. Technol.* **14** 722–33
Hernandez-Avila J, Basurto E and de Urquijo J 2002 Electron transport and swarm parameters in CO_2 and its mixtures with SF_6 *J. Phys. D: Appl. Phys.* **35** 2264–9
Holstein T 1946 Energy distribution of electrons in high frequency gas discharges *Phys. Rev.* **70** 367–84
Janalizadeh R and Pasko V P 2020 A framework for efficient calculation of photoionization and photodetachment rates with application to the lower ionosphere *J. Geophys. Res.: Space Phys.* **125** e2020JA027979
Janalizadeh R and Pasko V P 2023 Preliminary modeling of magnetized sprite streamers on Jupiter following Juno's observations of possible transient luminous events *J. Geophys. Res.: Space Phys.* **128** e2022JA031009
Jánský J and Pasko V P 2020 Modeling of streamer ignition and propagation in the system of two approaching hydrometeors *J. Geophys. Res.: Atmos.* **125** e2019JD031337
Kabirzadeh R, Lehtinen N G and Inan U S 2015 Latitudinal dependence static mesospheric E fields above thunderstorms *Geophys. Res. Lett.* **42** 4208–15
Kuo C-L *et al* 2007 Modeling elves observed by FORMOSAT-2 satellite *J. Geophys. Res.: Space Phys.* **112** A11312

Liu N, Dwyer J R and Cummer S A 2017 Elves accompanying terrestrial gamma ray flashes *J. Geophys. Res.: Space Phys.* **122** 10563–76

Loureiro J and Amorim J 2016 *Kinetics and Spectroscopy of Low Temperature Plasmas* (Berlin: Springer)

Marshall R A 2009 Very low frequency radio signatures of transient luminous events above thunderstorms *PhD Thesis* Stanford University

Marshall R A, Inan U S and Glukhov V S 2010 Elves and associated electron density changes due to cloud-to-ground and in-cloud lightning discharges *J. Geophys. Res.: Space Phys.* **115** A00E17

Morgan W L and Penetrante B M 1990 ELENDIF: a time-dependent Boltzmann solver for partially ionized plasmas *Comput. Phys. Commun.* **58** 127–52

Morrow R and Lowke J J 1997 Streamer propagation in air *J. Phys. D: Appl. Phys.* **30** 614–27

Moss G D, Pasko V P, Liu N Y and Veronis G 2006 Monte Carlo model for analysis of thermal runaway electrons in streamer tips in transient luminous events and streamer zones of lightning leaders *J. Geophys. Res.: Space Phys.* **111** A02307

Nagano I, Yagitani S, Miyamura K and Makino S 2003 Full-wave analysis of elves created by lightning-generated electromagnetic pulses *J. Atmos. Sol.-Terr. Phys.* **65** 615–25

Pasko V P, Inan U S and Bell T F 1998 Ionospheric effects due to electrostatic thundercloud fields *J. Atmos. Sol.-Terr. Phys.* **60** 863–70

Pérez-Invernón F J, Luque A and Gordillo-Vázquez F J 2018 Modeling the chemical impact and the optical emissions produced by lightning-induced electromagnetic fields in the upper atmosphere: the case of halos and elves triggered by different lightning discharges *J. Geophys. Res.: Atmos.* **123** 7615–41

Raizer Y P 1991 *Gas Discharge Physics* (New York: Springer)

Salem M A, Liu N and Rassoul H K 2016 Modification of the lower ionospheric conductivity by thunderstorm electrostatic fields *Geophys. Res. Lett.* **43** 5–12

Seeger M, Avaheden J, Pancheshnyi S and Votteler T 2016 Streamer parameters and breakdown in CO_2 *J. Phys. D: Appl. Phys.* **50** 015207

Starikovskiy A Y, Aleksandrov N L and Shneider M N 2021 Streamer self-focusing in an external longitudinal magnetic field *Phys. Rev.* E **103** 063201

Tonev P and Velinov P 2016 Vertical coupling between troposphere and lower ionosphere by electric currents and fields at equatorial latitudes *J. Atmos. Sol.-Terr. Phys.* **141** 39–47

Veronis G, Pasko V P and Inan U S 2001 Characteristics of mesospheric optical emissions produced by lightning discharges *J. Geophys. Res.: Space Phys.* **104** 12645–56

Plasma Sources Science and Technology
Supplementary file for

Efficient modeling of electron kinetics under influence of externally applied electric field in magnetized weakly ionized plasma

Reza Janalizadeh, Zaid Pervez, and Victor P. Pasko
Communications and Space Sciences Laboratory, Department of Electrical Engineering, The Pennsylvania State University, University Park, PA 16802, United States of America

4 May 2023

Contents

List of Figures

1. Two-dimensional (2D) error plots for the approximate transcendental method

Figure S1 shows 2D plots presenting the percentage error of the proposed approximate transcendental method compared to exact solution calculated by BOLSIG+ when $\vec{B} \neq 0$ for air and electron mean energy ε_{m}, electron impact ionization frequency ν_{i}, electron mobility parallel to magnetic field $\mu_{\parallel}$, and electron mobility perpendicular to magnetic field $\mu_{\perp}$, as functions of the angle $\angle\vec{E},\vec{B}$ and reduced electron gyrofrequency ω_{ce}/N, for selected values of reduced applied electric field E/N. Figures S2 and S3 show the corresponding plots for a a mixture of 88% H_2 and 12% He, and pure CO_2, respectively. The values selected for the reduced field E/N for each gas are $0.5E_{\mathrm{k}}$, E_{k}, and $1.5E_{\mathrm{k}}$, where E_{k} is the breakdown field for the gas, equal to $\sim$ 120, 40, and 80 Td respectively for air, mixture of 88% H_2 and 12% He, and pure CO_2. The proposed method provides good results for all the electron rate and transport coefficients shown, except for the ionization frequency ν_{i}. We note that the error is quite low for ε_{m}, $\mu_{\parallel}$, and $\mu_{\perp}$ for all three gas mixtures throughout the considered range of input parameters $(E/N, \omega_{\mathrm{ce}}/N, \angle\vec{E},\vec{B})$, except for very small regions in the upper right quadrants, which is expected as one moves from the regime of non-magnetized ($\beta_{\mathrm{eff}} \ll 1$) to highly magnetized ($\beta_{\mathrm{eff}} \gg 1$) plasma, i.e, as ω_{ce}/N approaches 10^{-12} rad m^3 s^{-1}, and $\angle\vec{E},\vec{B}$ approaches 90°. Significantly larger errors are seen for the electron impact ionization frequency ν_{i} for all three gases, and the error becomes considerable as we move towards the upper right quadrants. However, as already addressed in the paper, in a realistic scenario where ω_{ce}/N and $\angle\vec{E},\vec{B}$ may vary in the entire range shown, ν_{i} values corresponding to high ω_{ce}/N and large $\angle\vec{E},\vec{B}$ are so insignificant that the large error has no practical significance in the framework of plasma fluid models in which these coefficients are typically employed. The white spaces in these panels correspond to regimes where the plasma is highly magnetized such that ν_{i} is identically zero. We further note that for the panel corresponding to ν_{i} in the 88% H_2 and 12% He mixture at $E/N = 20$ Td, on account of the low electric field, ν_{i} is practically zero almost everywhere, and we used a much higher precision in our BOLSIG+ calculations than the default value to plot the ν_{i} panels shown.

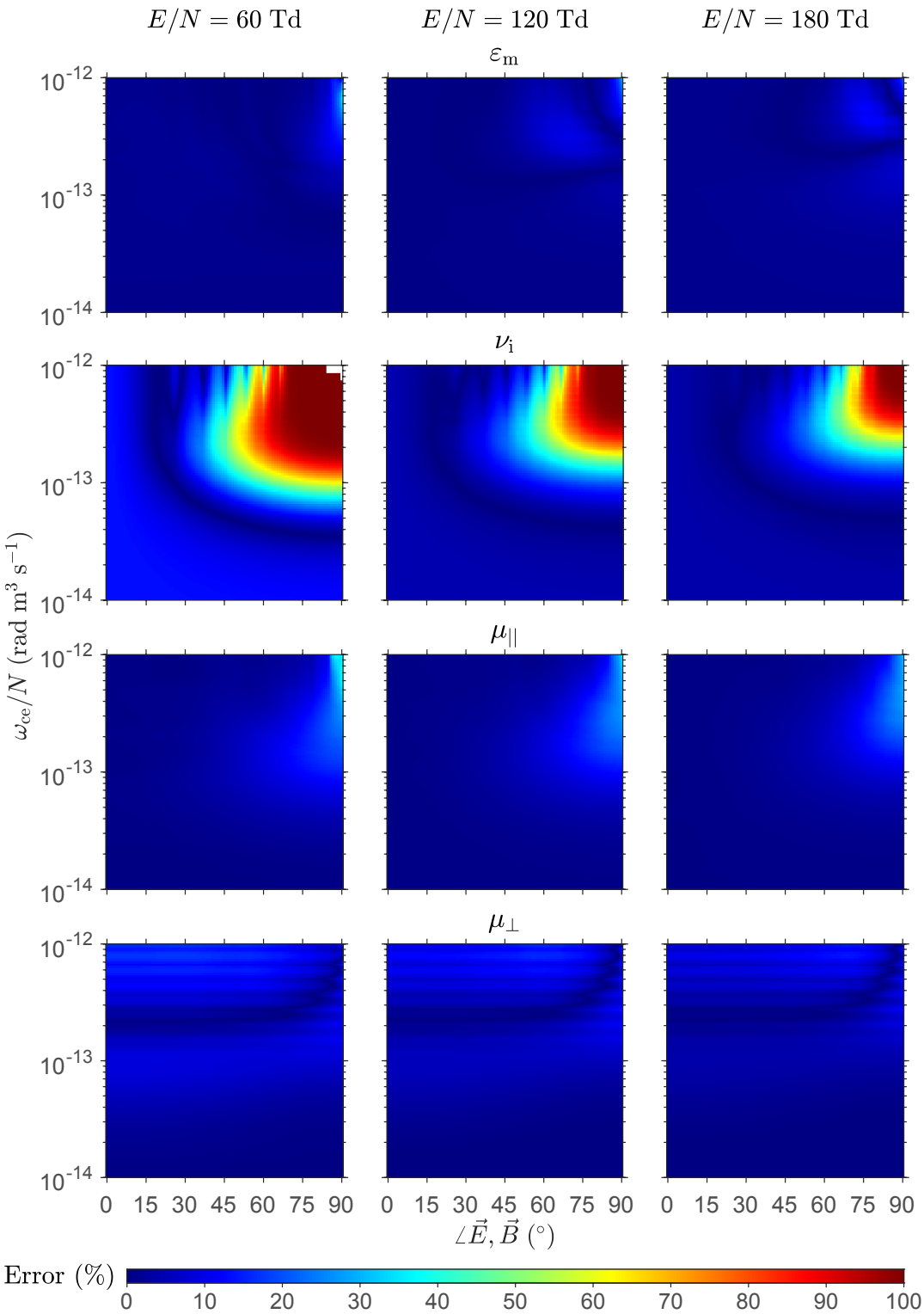

Figure S1: Percentage error of proposed transcendental method in approximate form for electron mean energy ε_{m}, electron impact ionization frequency ν_{i}, electron mobility parallel to magnetic field $\mu_{||}$, and electron mobility perpendicular to magnetic field $\mu_{\perp}$, as a function of the angle $\angle\vec{E},\vec{B}$ and reduced electron gyrofrequency ω_{ce}/N, for selected values of applied reduced electric field E/N. Results are for air.

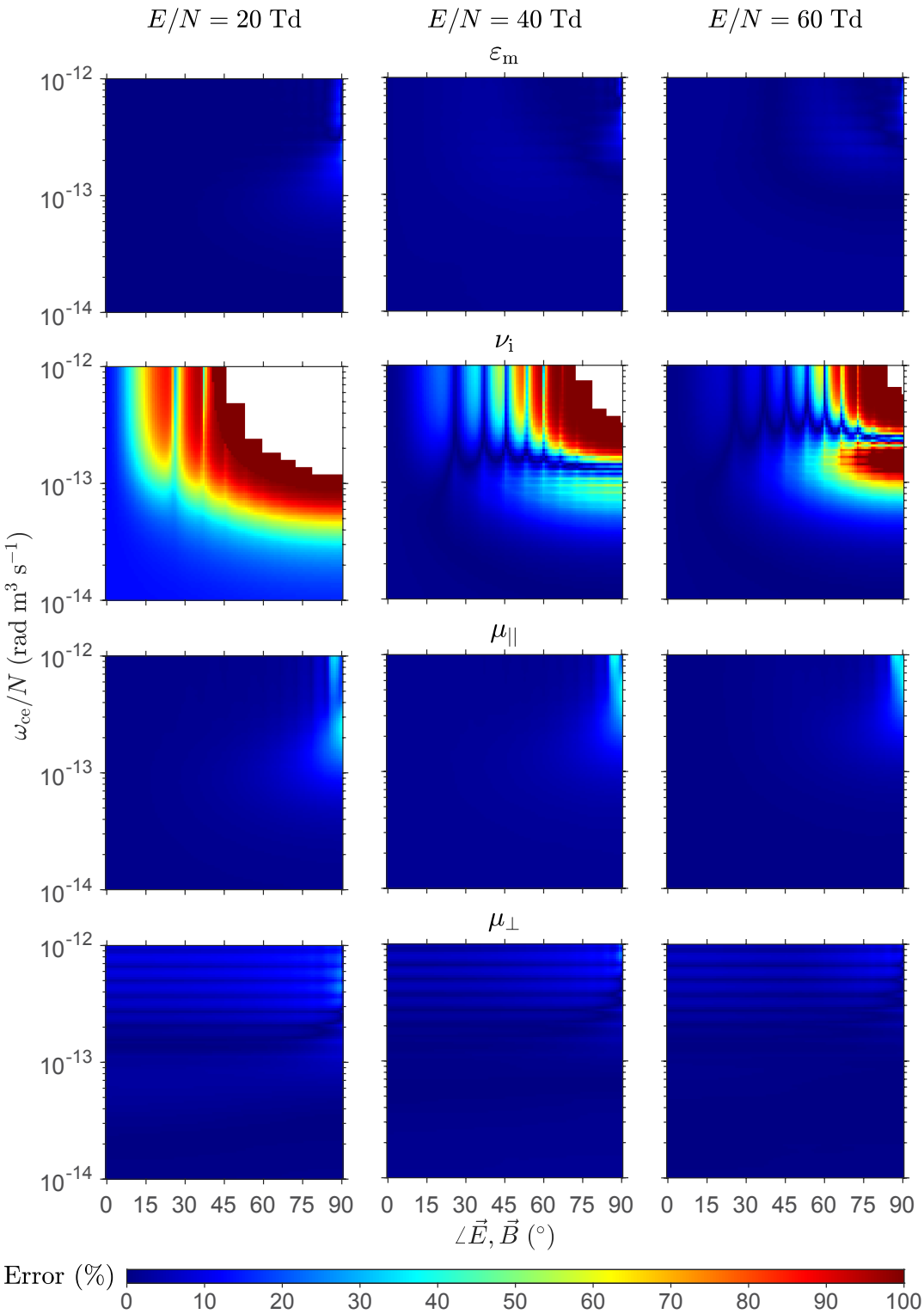

Figure S2: Percentage error of proposed transcendental method in approximate form for electron mean energy ε_{m}, electron impact ionization frequency ν_{i}, electron mobility parallel to magnetic field $\mu_{\parallel}$, and electron mobility perpendicular to magnetic field $\mu_{\perp}$, as a functions of the angle $\angle\vec{E},\vec{B}$ and reduced electron gyrofrequency ω_{ce}/N, for selected values of applied reduced electric field E/N. Results are for a mixture of 88% H_2 and 12% He.

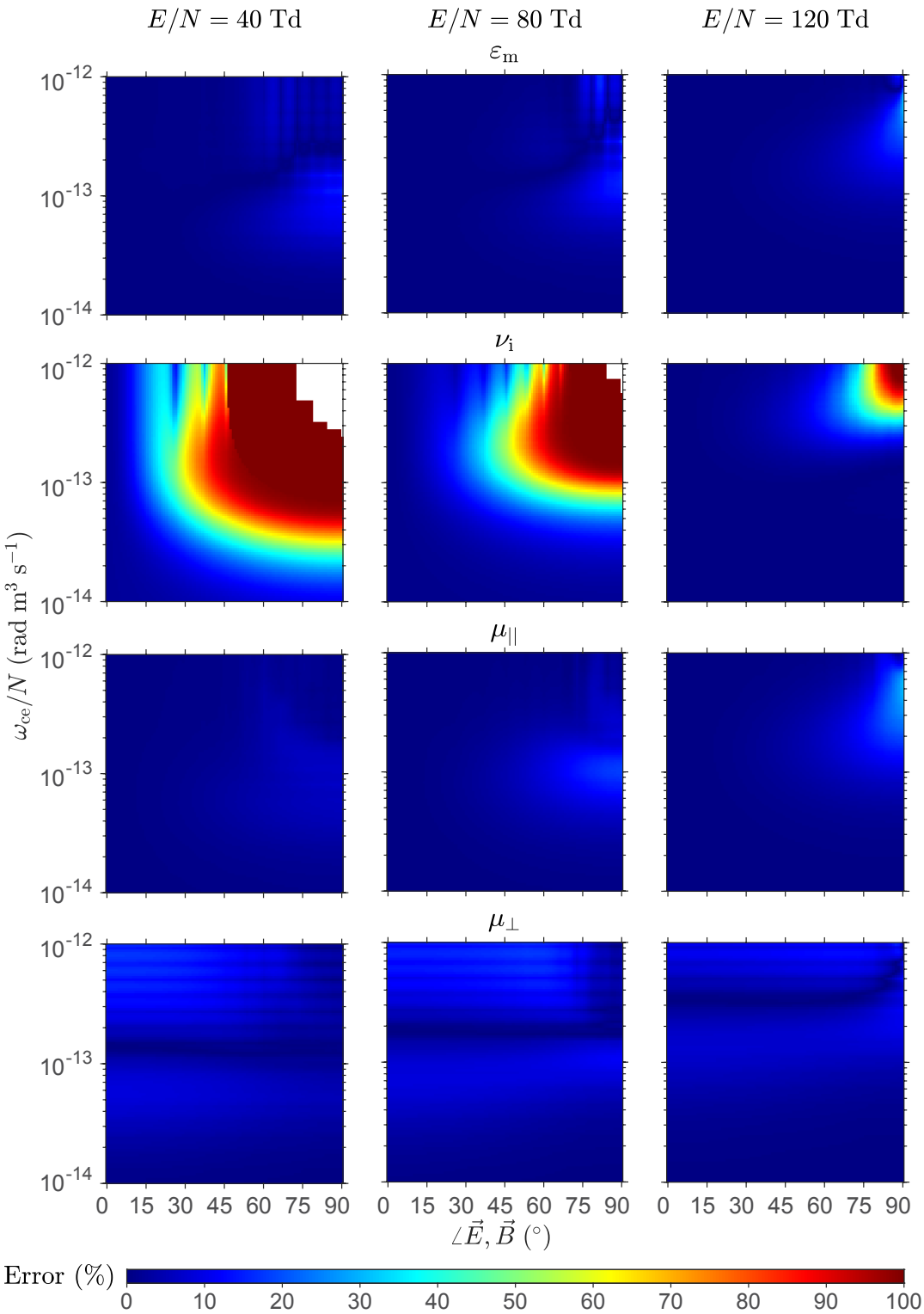

Figure S3: Percentage error of proposed transcendental method in approximate form for electron mean energy ε_{m}, electron impact ionization frequency ν_{i}, electron mobility parallel to magnetic field $\mu_{||}$, and electron mobility perpendicular to magnetic field $\mu_{\perp}$, as a function of the angle $\angle\vec{E},\vec{B}$ and reduced electron gyrofrequency ω_{ce}/N, for selected values of applied reduced electric field E/N. Results are for pure CO_2.

2. Convergence of the proposed transcendental method

Following Appendix E of the paper, where we already discussed the existence and uniqueness of the solution to the proposed transcendental method, we show here that the fixed point iteration method always converges to the solution for the gas mixtures presented in this study, provided a judicious choice of the the initial value x_0 is made to start the iterations. We solve for x in the equation $x = \phi(x)$, where $x = E_{\text{eff}}/N$, and $\phi(x) = \frac{1}{N}\left[E_{\parallel}^2 + \frac{E_{\perp}^2}{1+\beta^2(x)}\right]^{1/2}$. The condition for convergence is given by the Fixed Point Theorem [Burden and Faires, 2005, p. 58-59, Theorem 2.3] which states that if $\phi \in C[a,b]$ (where $C[a,b]$ is the space of all continuous functions in the interval $[a,b]$) such that $\phi(x) \in [a,b]$, for all x in $[a,b]$ and if, in addition, ϕ' exists on (a,b) and a positive constant $k < 1$ exists such that

$$|\phi'(x)| \leq k, \quad \text{for all } x \in (a,b), \tag{1}$$

then for any number x_0 in $[a,b]$, the sequence defined by

$$x_{n+1} = \phi(x_n), \quad \text{where } n = 0, 1, 2, \ldots \tag{2}$$

converges to the unique fixed point x in $[a,b]$. Since the function ϕ is indeed continuous, and $\phi(x) \in [0, E/N]$, for all x in $[0, E/N]$, where $E = \sqrt{E_{\parallel}^2 + E_{\perp}^2}$, we only need to check condition (1) for convergence.

Consider the problem of calculating E_{eff}/N in pure CO_2 gas. We assume the worst-case scenario in terms of the performance of the transcendental method where $\angle\vec{E}, \vec{B} = 90°$, i.e., $E_{\parallel} = 0$ and $E_{\perp} = E$, since this is when the effect of the magnetic field is strongest and results in the highest reduction of E_{eff} compared to E. Thus,

$$\phi(x) = \frac{E/N}{[1+\beta^2(x)]^{1/2}}. \tag{3}$$

We consider solutions for three values of the magnetic field (or equivalently, the reduced electron cyclotron frequency ω_{ce}/N), where $(\omega_{\text{ce}}/N)_1 = 10^{-14}$ rad m^2 s^{-1} corresponds to weakly magnetized electrons ($\beta \ll 1$), $(\omega_{\text{ce}}/N)_2 = 10^{-13}$ rad m^2 s^{-1} corresponds to partially magnetized electrons ($\beta \sim 1$), and $(\omega_{\text{ce}}/N)_3 = 10^{-12}$ rad m^2 s^{-1} corresponds to highly magnetized electrons ($\beta \gg 1$). In addition we consider three representative values of the applied field for each case, i.e., $E/N = 10$, 100, and 1000 Td.

Figure S4 shows $\phi(x)$ and $|d\phi/dx|$ as functions of x for all three values of E/N and for each value of ω_{ce}/N considered. A dashed line representing $y = x$ is also shown. Graphically, we can determine the root as the intersection of $\phi(x)$ with $y = x$. We note that for the weakly magnetized case, i.e., $(\omega_{\text{ce}}/N)_1$, condition (1) is satisfied for all three values of E/N (Figure S4(b)), which ensures both the uniqueness of the solution, and convergence of the fixed-point iteration method to the unique fixed-point. For the partially magnetized case, i.e., $(\omega_{\text{ce}}/N)_2$, condition (1) is still satisfied for $E/N = 10$ Td, but it is not satisfied for $E/N = 100$ and 1000 Td (Figure S4(d)) in the entire range

of $[0, E/N]$. However, we note that for $E/N = 100$ Td, condition (1) is satisfied for $x \in [\simeq 20 \text{ Td}, E/N]$. So we conclude that a unique root does exist in the range $[\simeq 20 \text{ Td}, E/N]$. We further confirm graphically from Figure S4(c) that this root indeed exists, and is unique not only in $[\simeq 20 \text{ Td}, E/N]$, but in the entire range $[0, E/N]$. We note that due to the log scale chosen for plotting, Figure S4(c) only shows $x \in [1, 1000]$ Td. It is easy to check that the root is indeed unique in $[0, E/N]$. Similarly, for $E/N = 1000$ Td, condition (1) is satisfied for $x \in [\sim 120 \text{ Td}, E/N]$ and a unique root exists in this range. For the highly magnetized case, i.e., $(\omega_{ce}/N)_3$, condition (1) is satisfied for $E/N = 10$ and 100 Td, and hence a unique root exists. For $E/N = 1000$ Td, condition (1) is satisfied for $x \in [\simeq 60 \text{ Td}, E/N]$, and we conclude, following a similar discussion as for the partially magnetized case, that a unique root exists.

We hence conclude that a unique solution to equation (E.1) exists for the wide range of values of magnetic field and applied electric field presented. We further note that $|d\phi/dx|$ becomes smaller as x becomes larger, such that x_0 should be chosen to lie towards the upper bound of the $[0, E/N]$ interval to ensure that condition (1) is satisfied (see Figures S4, S5, and S6). Further, it is recommended that x_0 be chosen such that it is greater than the solution x. Although this x is not known initially, we know that $x \leq E/N$, and hence, a simple choice that always satisfies this condition is $x_0 = E/N$, and we note that this choice always led to convergence in tests conducted. Corresponding results for air, and the (88% H_2, 12% He) mixture resembling Jupiter's atmosphere are presented in Figures S5 and S6, respectively. An analysis similar to that of CO_2 leads to the same conclusion, that is, the fixed-point iteration method converges to a unique solution for both air and the (88% H_2, 12% He) mixture in all cases. These conditions for convergence can be similarly checked for an arbitrary gas mixture of interest.

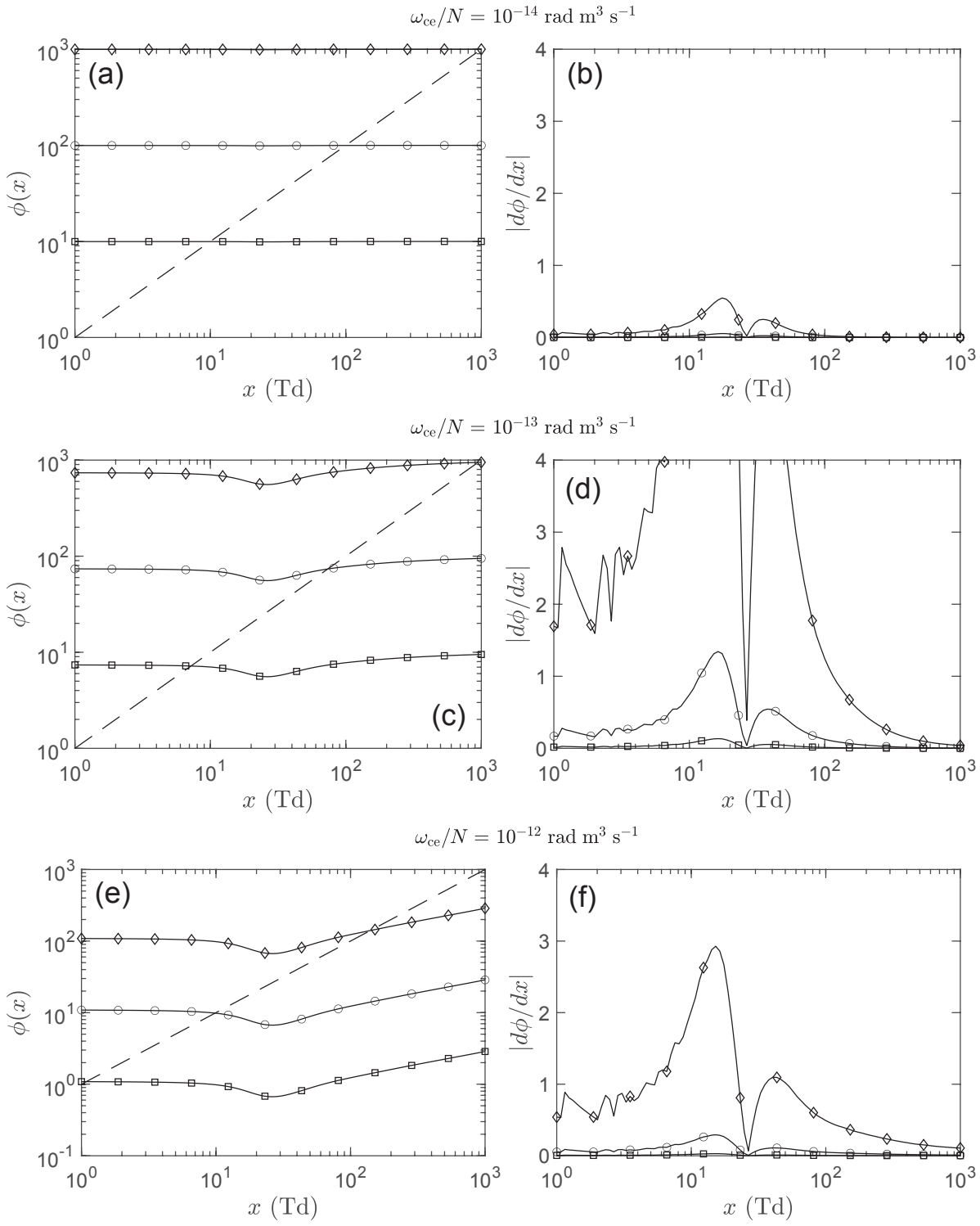

Figure S4: $\phi(x)$ and $|d\phi/dx|$ for weakly ($\omega_{ce}/N = 10^{-14}$ rad m^3 s^{-1}), partially ($\omega_{ce}/N = 10^{-13}$ rad m^3 s^{-1}), and highly ($\omega_{ce}/N = 10^{-12}$ rad m^3 s^{-1}) magnetized plasma in pure CO_2. The dashed line represents the $y = x$ line, and the intersection of $\phi(x)$ with this line is the root of the equation $x = \phi(x)$.

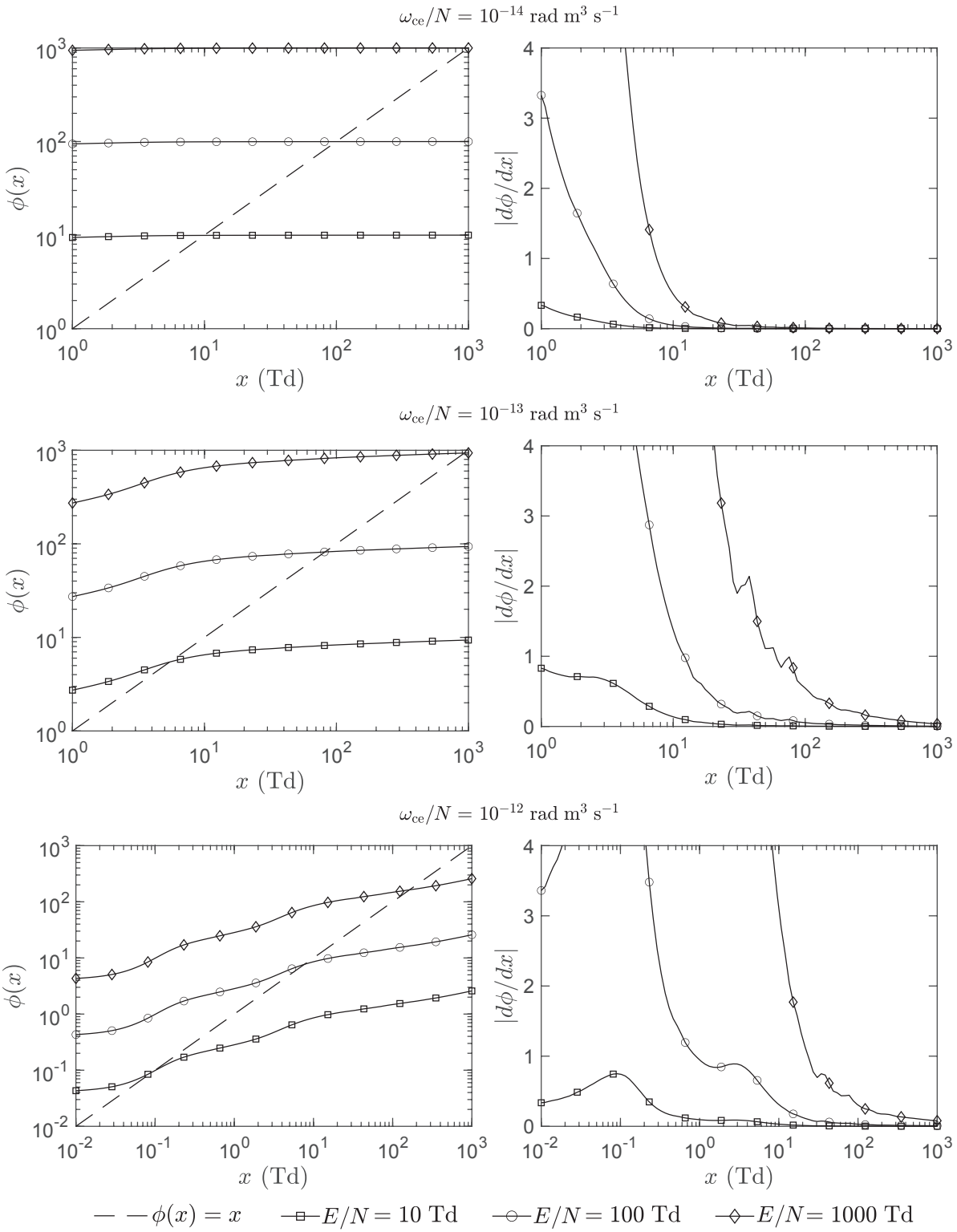

Figure S5: $\phi(x)$ and $|d\phi/dx|$ for weakly ($\omega_{ce}/N = 10^{-14}$ rad m^3 s^{-1}), partially ($\omega_{ce}/N = 10^{-13}$ rad m^3 s^{-1}), and highly ($\omega_{ce}/N = 10^{-12}$ rad m^3 s^{-1}) magnetized plasma in air. The dashed line represents the $y = x$ line, and the intersection of $\phi(x)$ with this line is the root of the equation $x = \phi(x)$.

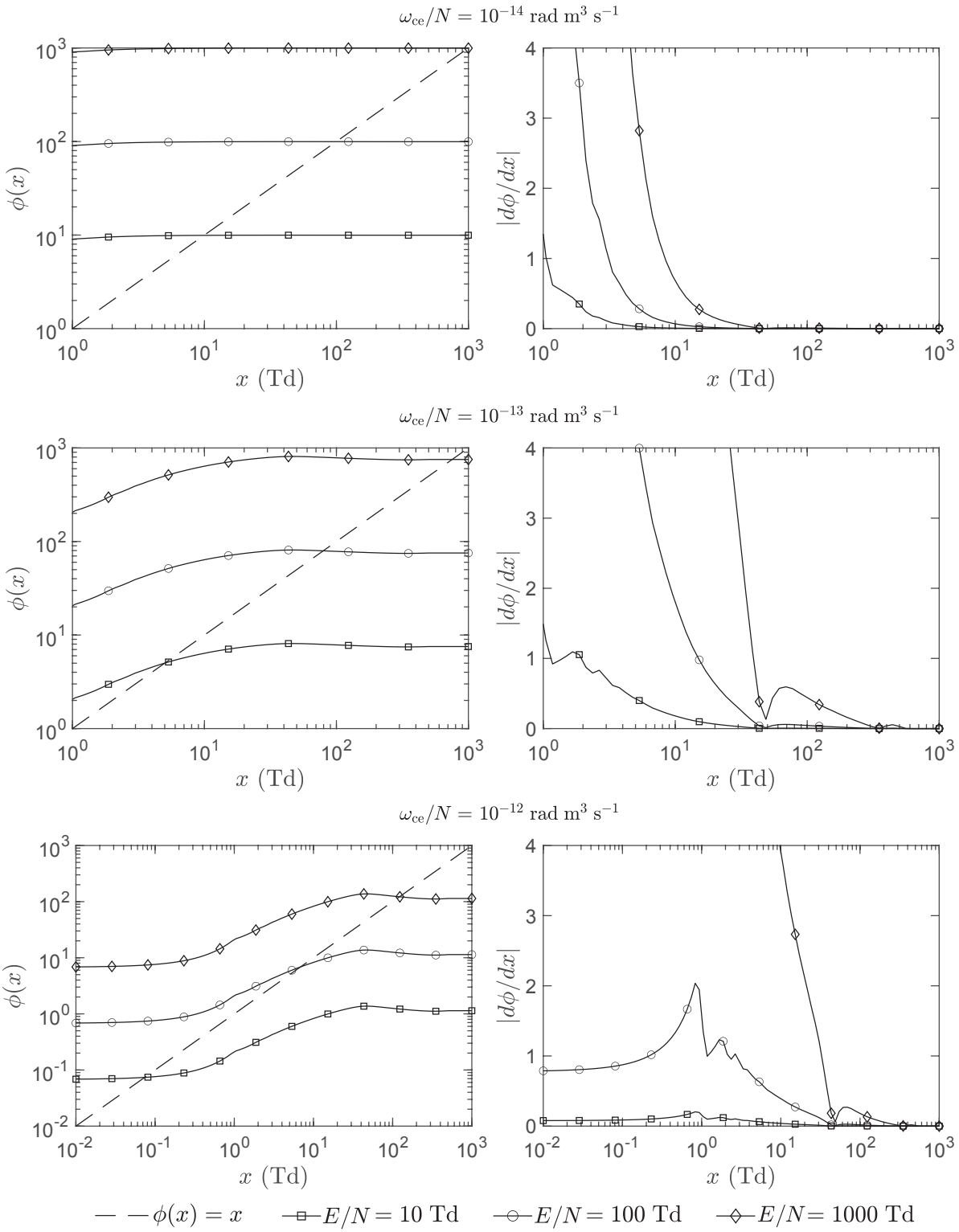

Figure S6: $\phi(x)$ and $|d\phi/dx|$ for weakly ($\omega_{ce}/N = 10^{-14}$ rad m^3 s^{-1}), partially ($\omega_{ce}/N = 10^{-13}$ rad m^3 s^{-1}), and highly ($\omega_{ce}/N = 10^{-12}$ rad m^3 s^{-1}) magnetized plasma in a mixture of 88% H_2 and 12% He. The dashed line represents the $y = x$ line, and the intersection of $\phi(x)$ with this line is the root of the equation $x = \phi(x)$.

References

R. L. Burden and J. D. Faires. *Numerical Analysis*. Thomson Brooks/Cole, Belmont, CA, eighth edition, 2005.